Deep-Sea Research II ▮ (▮▮▮▮) ▮▮▮–▮▮▮

Contents lists available at ScienceDirect

Deep-Sea Research II

journal homepage: www.elsevier.com/locate/dsr2

# Forecasting and reanalysis in the Monterey Bay/California Current region for the Autonomous Ocean Sampling Network-II experiment

P.J. Haley Jr.[a,b,*], P.F.J. Lermusiaux[a,b,*], A.R. Robinson[b], W.G. Leslie[a,b], O. Logoutov[a,b], G. Cossarini[c,d], X.S. Liang[e,b], P. Moreno[f,b], S.R. Ramp[g], J.D. Doyle[h], J. Bellingham[g], F. Chavez[g], S. Johnston[i]

[a] Massachusetts Institute of Technology, 77 Mass. Avenue, Cambridge, MA 02139, USA
[b] Harvard University, 29 Oxford Street, Cambridge, MA 02138, USA
[c] Istituto Nazionale di Oceanografia e di Geofisica Sperimentale, Borgo Grotta Gigante 42/C, 34010, Sgonico (TS), Italy
[d] University of Trieste, Piazzale Europa, 1 I-34127, Trieste, Italy
[e] Courant Institute, 231 Mercer Street, New York, NY 10012, USA
[f] Swedish Meteorological and Hydrological Institute, Sven Källfelts gata 15 426 71 Västra Frölunda, Sweden
[g] Monterey Bay Aquarium Research Institute, 7700 Sandholdt Road, Moss Landing, CA 95039, USA
[h] Naval Research Laboratory, 7 Grace Hopper Avenue, Monterey, CA 93943, USA
[i] Scripps Institution of Oceanography, 9500 Gilman Drive, La Jolla, CA 92093, USA

ARTICLE INFO

*Article history:*
Accepted 15 August 2008

*PACS:*
92.10.Zf
92.10.ak
92.10.ah

*Keywords:*
Coastal upwelling
Data assimilation
Physical oceanography
Prediction
Skill
Uncertainty

ABSTRACT

During the August–September 2003 Autonomous Ocean Sampling Network-II experiment, the Harvard Ocean Prediction System (HOPS) and Error Subspace Statistical Estimation (ESSE) system were utilized in real-time to forecast physical fields and uncertainties, assimilate various ocean measurements (CTD, AUVs, gliders and SST data), provide suggestions for adaptive sampling, and guide dynamical investigations. The qualitative evaluations of the forecasts showed that many of the surface ocean features were predicted, but that their detailed positions and shapes were less accurate. The root-mean-square errors of the real-time forecasts showed that the forecasts had skill out to two days. Mean one-day forecast temperature RMS error was 0.26 °C less than persistence RMS error. Mean two-day forecast temperature RMS error was 0.13 °C less than persistence RMS error. Mean one- or two-day salinity RMS error was 0.036 PSU less than persistence RMS error. The real-time skill in the surface was found to be greater than the skill at depth. Pattern correlation coefficient comparisons showed, on average, greater skill than the RMS errors. For simulations lasting 10 or more days, uncertainties in the boundaries could lead to errors in the Monterey Bay region.

Following the real-time experiment, a reanalysis was performed in which improvements were made in the selection of model parameters and in the open-boundary conditions. The result of the reanalysis was improved long-term stability of the simulations and improved quantitative skill, especially the skill in the main thermocline (RMS simulation error 1 °C less than persistence RMS error out to five days). This allowed for an improved description of the ocean features. During the experiment there were two-week to 10-day long upwelling events. Two types of upwelling events were observed: one with plumes extending westward at point Año Nuevo (AN) and Point Sur (PS); the other with a thinner band of upwelled water parallel to the coast and across Monterey Bay. During strong upwelling events the flows in the upper 10–20 m had scales similar to atmospheric scales. During relaxation, kinetic energy becomes available and leads to the development of mesoscale features. At 100–300 m depths, broad northward flows were observed, sometimes with a coastal branch following topographic features. An anticyclone was often observed in the subsurface fields in the mouth of Monterey Bay.



## 1. Introduction

A large Office of Naval Research (ONR)-sponsored, multi-institution coastal predictive skill exercise, the Autonomous Ocean Sampling Network-II (AOSN-II),[1] occurred in August 2003 in the Monterey Bay region off central California. The goal of this exercise was to initiate at-sea research of an adaptive observing and prediction system, with the intent to assimilate various data types, adapt the deployment of platforms and allow the relocation

* Corresponding authors at: Massachusetts Institute of Technology, 77 Mass. Avenue, Cambridge, MA 02139, USA.
*E-mail addresses:* phaley@mit.edu (P.J. Haley Jr.), pierrel@mit.edu (P.F.J. Lermusiaux).

[1] http://www.mbari.org/aosn. Also see Curtin et al. (1993) and Curtin and Bellingham (2001).

0967-0645/$ - see front matter © 2008 Elsevier Ltd. All rights reserved.
doi:10.1016/j.dsr2.2008.08.010

of the system to other regions (Bellingham and Zhang, 2005). As described in this special issue (Ramp et al., 2009; Curtin and Bellingham, 2009; Davis et al., 2009), remote and *in situ* sensors and platforms were employed, including gliders (Davis et al., 2002; Rudnick et al., 2004; Shulman et al., 2009), drifters (Chavez et al., 1997), moorings, autonomous underwater vehicles (AUVs), research vessels and satellites and coastal radar (Shulman and Paduan, 2009) for remote sensing. The collection of such a dataset, with the intensive successful operations of two fleets of gliders and low-flying aircraft in coordination with vehicle control algorithms (Leonard and Graver, 2001; Fiorelli et al., 2006; Leonard et al., 2007; Davis et al., 2009) and two modeling systems, is unprecedented in oceanography (Bellingham, 2006). The present manuscript reports the real-time modeling research carried out with the Harvard Ocean Prediction System (HOPS; Robinson et al., 2002). For details of the use of the second modeling system (Rutgers Ocean Modeling System (ROMS)—West; Wang et al., 2005; Li et al., 2006) during AOSN-II, the reader is referred to Chao et al. (2009).

HOPS is an interdisciplinary ocean modeling system primarily designed for regional applications with modular schemes for rapid set-up, data assimilation and dynamical studies (Robinson et al., 1996; Robinson, 1999; Haley et al., 1999). The heart of HOPS is a physical primitive-equation (PE) dynamical model (Cushman-Roisin, 1994; Bryan, 1969), which is supported by topography conditioning software, data processing and gridding routines, initialization and assimilation schemes (Robinson et al., 1998), dynamical studies schemes, and visualization software. During AOSN-II, HOPS assimilated the various data types mentioned above and carried out predictions of ocean temperature, salinity and velocity fields over two–three days. ESSE (Lermusiaux et al., 2002) is a system for the distributed prediction of oceanic uncertainties and assimilation of various data types. ESSE schemes (Lermusiaux, 2006) are based on an ensemble approach for the error prediction, on a reduction of the error space to a dominant subspace, and on Kalman filtering and smoothing updates for the assimilation. During AOSN-II, they were used to carry out ensembles of nonlinear stochastic forecasts of physical fields and uncertainties (Lermusiaux, 2006, 2007; Lermusiaux et al., 2006) and to assimilate various data types. In total, 24 sets of real-time nowcasts and forecasts were released from 4 August to 3 September. The forecasts were forced by 3 km and hourly ocean-atmosphere flux predictions obtained from the U.S. Navy's operational Coupled Ocean/Atmosphere Mesoscale Prediction System (COAMPS, Doyle et al., 2009). The ocean observations collected were quality controlled and mapped by objective analysis (OA) daily. Boundary conditions and model parameters for atmospheric forcing were calibrated and modified in real-time to adapt to the evolving ocean conditions. Products were distributed on the Web, oceanic features and uncertainty fields were described, and adaptive sampling plans were provided on a daily basis.

The main features of the AOSN-II region are diagrammed in Fig. 1, along with the chosen HOPS modeling domains. These features were obtained from a study of the literature and from the results of the AOSN-II exercise. They are the: (1) upwelling centers at point Ano Nuevo (AN) and point Sur (PS), with the upwelled water advected equatorward and seaward (Huyer, 1983; Rosenfeld et al., 1994; Traganza et al., 1981; Ramp et al., 2005); (2) coastal current, eddies, squirts and filaments including the upwelling-induced jets and high (sub)-mesoscale variability in the Coastal Transition Zone (Brink et al., 1991; Huyer et al., 1991; Kosro et al., 1991; Strub et al., 1991; Ramp et al., 1991; Hayward and Mantyla, 1990; Chavez et al., 1991; Chavez and Collins, 2000); (3) California Undercurrent (CUC), which is a poleward flow/jet often found

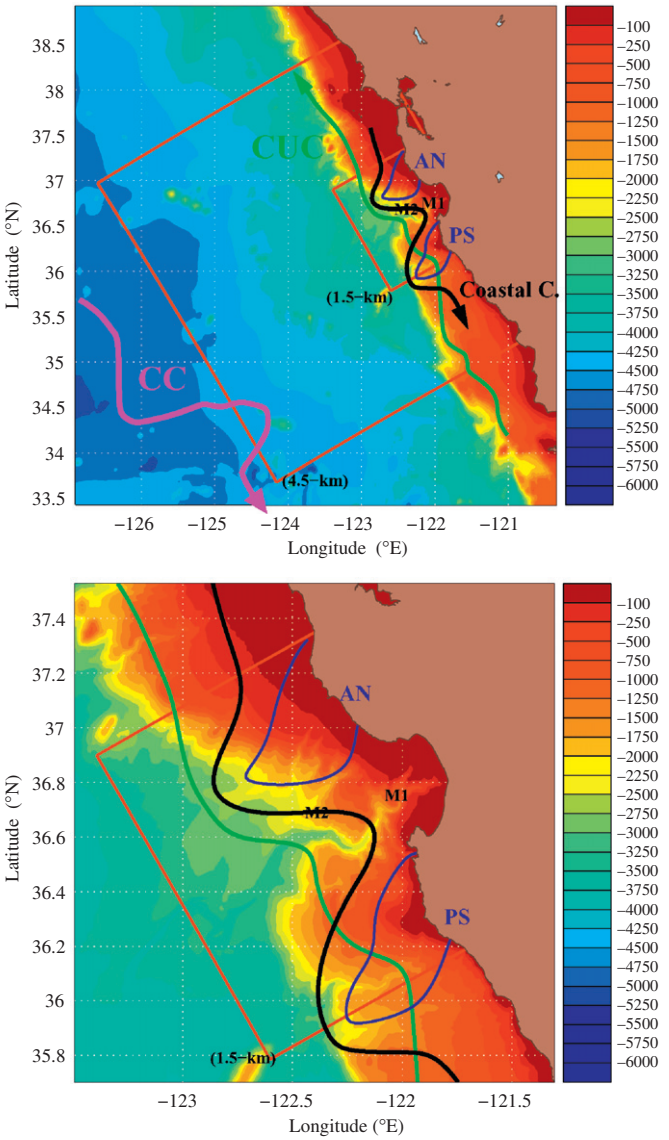


**Fig. 1.** Modeling domains for AOSN-II with bathymetry. Upper panel shows the "Data Domain" inside of the larger "Offshore Domain". Lower panel shows a zoom of the "Data Domain". Also shown are the main dynamical features: upwelling centers at point Año Nuevo (AN) and Point Sur (PS) (blue); coastal current, eddies, filaments, etc. (black); California Undercurrent (CUC) (green); California Current (CC) (magenta).

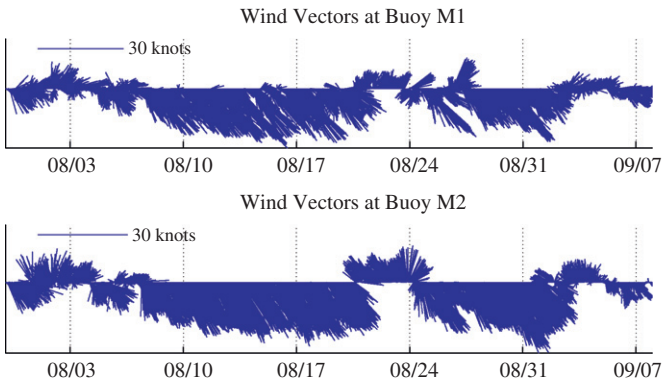


**Fig. 2.** Wind vectors (knots) at the M1 and M2 moorings (see Fig. 1 for mooring locations).

Please cite this article as: Haley, P.J. Jr., et al., Forecasting and reanalysis in the Monterey Bay/California Current region for the Autonomous Ocean Sampling Network-II experiment. Deep-Sea Research II (2008), doi:10.1016/j.dsr2.2008.08.010

10–100 km offshore and at 50–300 m depths (Collins et al., 1996; Garfield et al., 1999; Pierce et al., 2000; Wickham, 1975); (4) California Current (CC), a broad southward flow, often found 100–1350 km offshore and at 0–500 m depth (Collins et al., 2003; Huyer et al., 1998; Hickey, 1998; Marchesiello et al., 2003; Lynn and Simpson, 1987; Strub and James, 2000).

In the Monterey Bay region, the major external drivers of the surface ocean dynamics are atmospheric fluxes, especially the wind stress. In fact, these forcings define two different ocean states; classically known as upwelling and relaxation states (Rosenfeld et al., 1994). To provide a time line of these different events during AOSN-II, Fig. 2 shows the measured winds at the M1 and M2 moorings. In the period of August 8–17, both moorings show a sustained upwelling event, with a brief weakening around August 15. Between August 17 and 21, the more offshore M2 shows a continuation of upwelling-favorable winds while M1 indicates weakening and less uniformity in direction. The two moorings indicate a relaxation event between August 21 and 24. After, during August 24–27, M2 shows the start of another upwelling event but M1, closer to the shore, again shows less uniformity in direction. Between August 27 and September 1, the winds are generally in an upwelling-favorable direction, although the strength is falling off after August 29. Both moorings indicate a relaxation event between September 2 and 5.

Fig. 3 shows the positions of the main sources of *in situ* data used in this study. Three comprehensive CTD surveys were made by the R/V Pt. Sur (2–6 August; 21–25 August and 3–6 September 2003, Johnston et al., 2009). Each survey consisted of 58–69 CTD stations (69 for the first 2, 58 for the third) and, for the purposes of this study, each defined a natural time-window for constructing synoptic estimates of the ocean state. Also shown are the positions of the pseudo-profiles from the gliders. Scripps (SIO) maintained five gliders (Sherman et al., 2001) in the period 23 July–2 September, 2003; traveling yo-yo paths between the surface and 400 m. Woods Hole (WHOI) maintained 10 gliders in the period 21 July–31 August, 2003, sampling between the

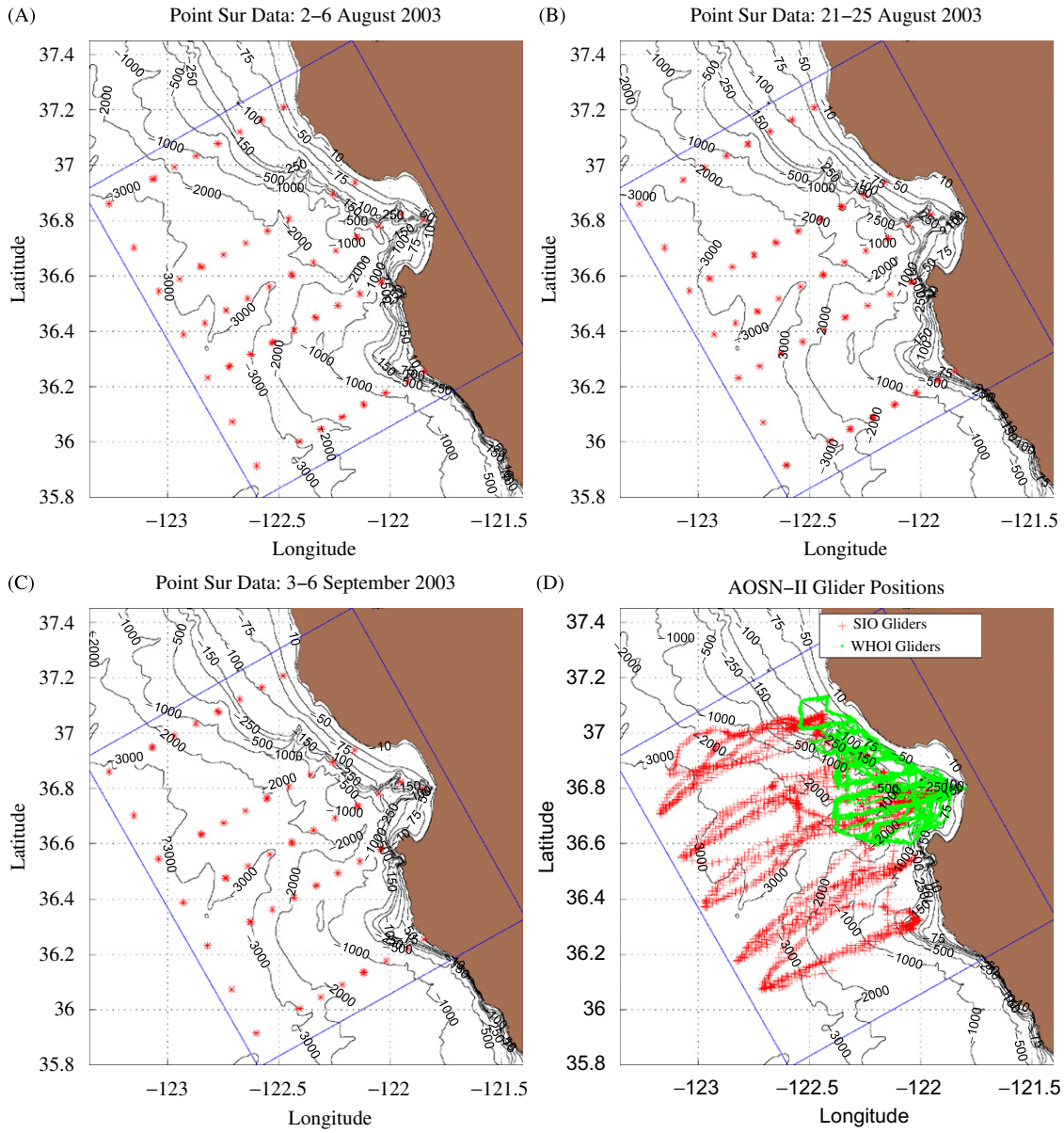


**Fig. 3.** Positions of primary sources of *in situ* data. (A–C) Locations of the R/V Pt. Sur (repeat) CTD surveys. (D) Locations of the pseudo-profiles from the Woods Hole and Scripps gliders.

Please cite this article as: Haley, P.J. Jr., et al., Forecasting and reanalysis in the Monterey Bay/California Current region for the Autonomous Ocean Sampling Network-II experiment. Deep-Sea Research II (2008), doi:10.1016/j.dsr2.2008.08.010

surface and 200 m. These gliders provided the bulk of the *in situ* ocean data (for more details of the AOSN-II glider operations, see Section 4 of Rudnick et al., 2004).

The two domains represented in Fig. 1 were designed to support two-way nested simulations. The innermost domain, referred to as the "Data Domain", contains the region of primary sampling around Monterey Bay, as well as the upwelling centers at point AN and PS. The larger domain, referred to as the "Off Shore Domain", provides a buffer for the Data Domain while capturing the longest expected plumes. The term "Data Domain" was chosen based on the AOSN-II sampling plans (Fig. 3).

During the exercise, the HOPS modeling was carried out in three different configurations. The first was the "Stand-alone Data Domain". In this case the PE model was configured to run in the Data Domain with open-boundary condition schemes (Section 2.3.4) utilized at the external boundaries. Data assimilation was done using the Optimal Interpolation (OI) method (Lozano et al., 1996; Lermusiaux, 1999). This configuration is always tried in a new region, so as to provide a modeling benchmark. Its relative simplicity facilitates a rapid search for a stable regime. The second configuration also used OI assimilation but was set for a two-way nested communication (Sloan, 1996; Spall and Holland, 1991; Fox and Maskell, 1995) between one model code set up for the Data Domain and another for the Off Shore Domain (see Appendix A for details). Theoretically, this provides a superior representation of the larger-scale lateral forcing on the smaller domain while simultaneously reducing boundary noise. However, if these larger-scale estimates are not sufficiently accurate, nesting can damage the fields in the smaller data-driven domain. During AOSN-II, there were no significant *in situ* data outside of the Data Domain and the larger-scale synoptic estimates were thus of limited reliability. It was only after shifting the GDEM[2] climatology (Davis et al., 1986) to the observed AOSN-II mean that the larger-scale Off Shore Domain was of some use. The third configuration was the "ESSE" configuration. This was essentially the "Stand-alone Data Domain" with assimilation being done via the ESSE. This configuration had a superior data assimilation methodology and also produced estimates of the forecast error. The forecasted error fields are not described in this manuscript. Although three model configurations were used, on a given day the issued forecast products came from a single configuration (except for August 12–13). One reason for this was that it was regarded by the other members of the AOSN-II team as confusing on the two days for which we issued from multiple sources. More importantly, we did not always have simultaneously useful forecasts from all configurations. As we tried new initialization schemes (Section 2.3.2) we would first find stable parameter regimes in the stand-alone OI configuration before attempting a nested configuration. At one point, the stand-alone ESSE configuration was being used for extensive parameter tuning, including new boundary conditions (Appendix B), following which only ESSE forecasts were available while the other configurations caught up.

## 2. Real-time approach, constraints and modeling system components

### 2.1. Approach

The chosen scientific approach sets the forecast methodologies and operational procedures. Our real-time approach is to: (i) initialize from a synoptic survey so as to capture the background ocean fields from the start; (ii) subsequently utilize as much ocean data as possible, both for skill evaluation and assimilation, (iii) keep some data out of the assimilation for sustained independent evaluations and, (iv) allow human intervention and carry out real-time scientific studies of the outputs prior to product dissemination. Detailed examination of each data-driven forecast output is not a guarantee of successful prediction but it is nonetheless essential. It involves studying, at a minimum, the evolution of the ocean fields for each forecast candidate at the depths and along the vertical sections that are dynamically key. For AOSN-II, this was mainly human-based but research is underway for autonomous scientific evaluations (Lermusiaux, 2007).

### 2.2. Constraints and operations

A main constraint on the above choices and approach is the ability to provide daily forecast products in a timely manner. This "timeliness" constraint is set by the available personnel and computing power.[3] For AOSN-II, the chosen procedure was to prepare a set of candidate forecasts each morning so as to include the most recent data and atmospheric forcings. The main timeliness constraint was that the forecasts needed to be finished, examined and have their products generated by late afternoon for the AOSN-II team teleconferences.

The canonical day's operations then proceeded as follows (see also Fig. 4). First, the most recent data and atmospheric forcings were gathered and processed for use in the HOPS PE model and ESSE ensemble predictions. An initialization was generated from the previous day's simulation, from the fields corresponding to 0000Z on the previous day. To calibrate numerical and dynamical model parameters to the region and data, several PE simulations would then be run, using the updated atmospheric forcings and assimilating the new data but with different model parameters. These simulations were then visually compared to available data (CTD, glider, aircraft and satellite SST, CODAR) assessing the evolution of the main features (depths of the thermocline and surface mixed layer, extent of any upwelling, and general circulation in Monterey Bay). The simulations also were inspected for the presence and extent of numerical error (e.g. errors originating at the open boundaries). The simulation with the best data match and minimal numerical error would then be selected and the corresponding forecast products generated and disseminated. There were two paths for the dissemination of HOPS products. The first was our local web page,[4] the second was the MBARI server.[5] Adaptive sampling recommendations were also provided to the AOSN-II team on a daily basis (see RTOC links in local web site). Their heuristic objectives were (i) to sample interesting features of the predicted dynamics, (ii) to reduce the predicted uncertainties of the ocean field estimates or (iii) to maintain coverage over the whole ocean region. Results from this adaptive sampling have been previously published by Lermusiaux (2007).

### 2.3. Modeling system components

In real-time regional ocean predictions, the choices made in setting up the modeling system for the dynamics of interest are essential. This is because a modeling system consists of a large number of components that need to be adequately selected given

[2] https://128.160.23.42/gdemv/gdemv.html

[3] For AOSN-II, we utilized a set of 10–18 distributed processors 4–6 years old and with 200–400 MHz clock speed.

[4] http://people.deas.harvard.edu/~leslie/AOSNII/

[5] http://www.mbari.org/aosn/AOSN_MB2003table.htm

Please cite this article as: Haley, P.J. Jr., et al., Forecasting and reanalysis in the Monterey Bay/California Current region for the Autonomous Ocean Sampling Network-II experiment. Deep-Sea Research II (2008), doi:10.1016/j.dsr2.2008.08.010

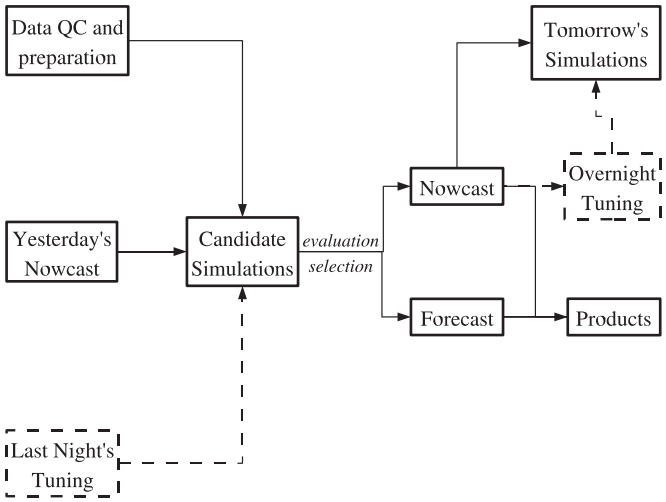


**Fig. 4.** Flowchart of the canonical day's operations for AOSN-II. The tuning operations (shown in dashed lined) were not performed in AOSN-II but were suggested by the reanalysis. These tunings are a form of adaptive modeling (Lermusiaux, 2007) in which a series of sensitivity studies are used to improve the parameterizations during the operation. This notion was successfully employed during the subsequent Monterey Bay 2006 experiment.

the constraints of the specific prediction exercise. The components of modeling systems include: the bathymetry, the domains (nesting, stand-alone, etc.), the numerical properties (scheme, grids, vertical and horizontal resolution, etc.), the data utilized, the initial conditions, the open and land boundary conditions, the forcings including atmospheric fluxes, tides and rivers, the data assimilation scheme, the chosen model dynamics, the dynamical parameterizations and finally, the dynamical and computational parameters. Some of these components are summarized next. Additional details are given in Appendix A.

### 2.3.1. Data

The data utilized for evaluation and assimilation consisted of measurements collected by gliders, aircraft, AUVs and ships (Ramp et al., 2009). The synoptic oceanographic data were evaluated, processed and objectively analyzed on a daily basis. The data were first visually inspected on an instrument by instrument basis to ensure internal consistency. In some cases, filtering was applied. After this first pass of quality control, data from different instruments were visually compared to each other. Outliers were identified and removed, retaining as much data as possible. Once the data had passed this quality control procedure, they were objectively analyzed (Bretherton et al., 1976; Carter and Robinson, 1987).

### 2.3.2. Initialization

For the AOSN-II region, the initial conditions were found to set the quality of the ocean predictions over days to weeks. This is, in a large part, related to the time required to modify the mean background state below the surface mixing layer and over the larger domain shown in Fig. 1. During the AOSN-II exercise, the initialization fields we utilized changed with time, according to the three R/V Pt. Sur surveys. Prior to August 7, the first R/V Pt. Sur survey data were not yet completed and processed. The forecasts issued in those times were initialized with July 2003 data combined with historical synoptic surveys. Three other initial conditions based on climatological data, El Niño data and La Niña data were also utilized, but none matched the synoptic data as it was collected. The July 2003 dataset was a better fit, but still not a very good one. In the period August 7–26, the processed first survey was available. The forecasts were then either directly re-initialized with this first survey or were restarts from forecasts that, ultimately, traced back to this initialization survey. After August 26, the second survey was processed and the forecasts were again either initialized from this second survey or from restarts that traced back to it. This applies to both the fields and to the uncertainty computations using ESSE. This re-initialization was useful to reduce the effects of uncertainties in open-boundary conditions which had been compounded for 3 weeks of forecasting from the previous survey.

### 2.3.3. Forcings

The atmospheric forcings for our AOSN-II HOPS simulations were generated based on the Navy's operational COAMPS (Hodur, 1997) analysis and 72-h forecast fields, received on a twice daily basis (Doyle et al., 2009). The COAMPS fields were available on four different resolution lambert conformal projection grids. The nominal 0.03° resolution fields were used to generate forcings for the Data Domain. The nominal 0.1° fields were used to generate forcings for the Offshore domain. Overall, it was found that these forcings were of a quality superior to anything we had utilized before. We also found that the 0.03° resolution forcing was necessary for ocean predictions of upwelling events at AN and PS. Finally, our AOSN-II simulations were not forced by tides nor by river inputs (Rosenfeld et al., 2009; Wang et al., 2009).

### 2.3.4. Parameterizations and parameters

In our general approach (Section 2.1), we usually test our system with relevant historical synoptic datasets before the real-time operation so as to estimate a range of adequate parameter values. In the six months prior to AOSN-II, we were provided with several datasets: June–August 2000 ICON PE model fields and atmospheric fluxes from Igor Shulman (Shulman et al., 2002); a May–June 1989 synoptic survey from Leslie Rosenfeld; as well as NODC and CalCOFI (Scripps Institution of Oceanography, 1999) data. Using these data with synoptic winds and process-oriented idealized winds (upwelling–relaxation cycles), we chose an initial set of dynamical and computational parameters for both numerical stability and dynamical response.

The parameterizations and parameter value ranges that were utilized during AOSN-II were as follows. All simulations were made with a 300-s time step. The lateral open boundary forcing was parameterized with the implicit Orlanski (1976) radiation condition for the tracer, velocity and transport streamfunction variables. For the rate of change of barotropic vorticity, the boundary condition most often used was a CFvN condition (Charney et al., 1950), recast for the PE by Spall and Robinson (1989). In the last third of the experiment, the Orlanski condition was used on vorticity. The horizontal sub-gridscale was parameterized by a Shapiro (1970) filter: a fourth-order filter was used for tracers and momentum, and a (stronger) second-order filter for the rate of change of barotropic vorticity. In the vertical, the background sub-gridscale was parameterized by a second-order diffusion term where the coefficients were functions of the Richardson number, as in Pacanowski and Philander (1981). The peak viscosity/diffusivity was set to $50\,cm^2/s$. The background viscosity and diffusivity were set in the range $0.1-0.2$ and $0.01-0.02\,cm^2/s$, respectively. Near the surface, vertical mixing (see Lermusiaux, 2001) is increased to at least $30\,cm^2/s$ for viscosity and $5-6\,cm^2/s$ for diffusivity, so as to reflect wind forcing. The depth to which these mixing bounds is applied is proportional to $(\|\tau\|/\rho_0)^{1/2}/f$ where $\tau$ is the wind stress, $\rho_0$ is the mean density of seawater and $f$ is the Coriolis factor. The non-dimensional constant of proportionality was set in the range 0.15–0.22. This wind mixing depth was never allowed to be shallower than 1 m or exceed 40 m. At depths where the water

Please cite this article as: Haley, P.J. Jr., et al., Forecasting and reanalysis in the Monterey Bay/California Current region for the Autonomous Ocean Sampling Network-II experiment. Deep-Sea Research II (2008), doi:10.1016/j.dsr2.2008.08.010

column is gravitationally unstable, the vertical viscosity/diffusivity were bounded from below by $50\,cm^2/s$. Finally, a Rayleigh friction parameterization of drag induced by the bottom or coasts (Lermusiaux, 1997) was used. In both cases, the temporal decay scale was 3600 s and the spatial decay was 1.5 (model levels from the bottom or grid points from the nearest coast, respectively).

#### 2.3.5. Data assimilation

The assimilation procedure was based on a daily cycle.[6] Once each simulation day, data were assimilated at a nominal assimilation time of 1200Z. Temperature and salinity data within ±18 h of that time were gathered and objectively analyzed with the assimilation scales in Table 1. These fields were then processed for the terrain-following coordinates, with a geostrophic internal mode velocity. These temperature, salinity and internal velocity fields were then assimilated into the model, according to their associated error fields. Rather than "shocking" the system by simply inserting the assimilation fields at the desired times, the fields are first assimilated earlier with down-weighted assimilation weights ("ramping in"). The schedule used, along with the down-weighting weights, is given in Table 2. As Table 2 indicates, we found out that the weights for assimilating the internal mode geostrophic velocity needed to be smaller than those for temperature and salinity, so as to not locally overwrite the PE physics with geostrophy. A weak assimilation after the center time (a "ramp out" cycle) was also included. Note that prior to August 19, the "ramp out" cycle was not used. Based on forecast evaluations, the weights for assimilating internal mode velocity were further decreased by a factor of 2, on August 19–21, and 28–30.

**Table 1**
Objective analysis correlation parameters

| | Initialization | | Assimilation | |
|---|---|---|---|---|
| | Synoptic | Mean | Synoptic | Mean |
| Decay (km) | 15 | 45 | 5 | 25 |
| Zero-cross (km) | 37.5 | 112.5 | 12.5 | 50 |
| Time-decay (day) | 10 | 1000 | 1 | 80 |

**Table 2**
Optimal Interpolation assimilation ramping parameters

| Time | Weights $(T,S)$ | Weights $(\vec{U}_{internal})$ |
|---|---|---|
| $t_{assim} - 0.25$ | 0.333 | 0.167 |
| $t_{assim} - 0.125$ | 0.666 | 0.333 |
| $t_{assim}$ | 0.999 | 0.5 |
| $t_{assim} + 0.25$ | 0.333 | 0.167 |

## 3. Real-time results

### 3.1. General circulation and hydrodynamics estimates

From August 4 to September 3, 2003, forecasts were issued on 23 days. Fig. 5 shows the temperature and velocity fields for 8 August 2003, which are illustrative of the state of the general circulation and hydrographic features during the entire period. This state was found to be in stronger-than-usual upwelling-favorable conditions (Ramp et al., 2009). Starting with the 30-m fields, the forecasts show a general cyclonic circulation in Monterey Bay, a situation we have found to occur during upwelling conditions. For significant upwelling conditions, a southward coastal current was often observed flowing along the shelf and across the mouth of Monterey Bay. Offshore, we observed an inflow in the western boundary, bending north and providing a general northward flow. This is indicative of a surfacing undercurrent, also referred to as the Davidson current (Brink et al., 1991). Inshore of this flow, but off the shelf, an anticyclonic eddy was usually present. The exact size, shape and position of this eddy was found to be fairly variable. The situation at the surface is very similar except during the periods of strong upwelling-favorable winds. In these periods, winds dominate, resulting in broad generally southward flow across the whole domain. The surface also shows a band of warmer water lining the coast of Monterey Bay, occasionally protruding out the northern edge of the mouth of the bay (not on August 8). This feature was sometimes in SST images. Our forecasts at times over-estimated the extent of the northward protrusion, in part due to fog conditions perhaps not fully represented in the atmospheric forcing fluxes but also in part due to flow fields that were too geostrophic. At 200-m, there is a general northward flow originating from the western boundary, sometimes accompanied by a northward branch along the slope, characteristic of the undercurrent. The eddy opposite Monterey Bay is still visible at this depth, sometimes even more so than at shallower depths.

Once the larger-scale initial conditions were estimated by the first R/V Pt. Sur survey, several uncertainties still remained in our (sub)-mesoscale predictions. This can be illustrated by predictions made by the three different PE configurations. Consider the forecasts that were issued on August 13th (Fig. 6). An important difference can be seen at 200 m (bottom row). Although the three cases show general northward flow, the stand-alone case has two distinct branches. The first enters from the western boundary and turns north. The second enters from the southern boundary by PS and flows north along the slope. This second branch pushes an eddy, originally opposite Monterey Bay, northward along the slope until, by August 13, it is opposite point AN. In contrast, the nested configuration has a large, anticyclonic half eddy on the southern boundary. This boundary eddy appears to choke off the along slope branch of the northward flow. As a result, the eddy that was originally opposite Monterey Bay does not advect nearly so far north by August 13. The inflow from the western boundary is broader and further south. It still bends north in a broad northward flow that fills most of the domain. The ESSE forecast is more similar to the stand-alone case, in that it has two branches. However, the inflow from the west is much broader for the ESSE forecast than the stand-alone OI forecast, covering the northern $\frac{2}{3}$ of the western boundary. Overall, the open boundary behaves better in the ESSE forecast than in the stand-alone OI forecast. Since the initial conditions were similar in the 144 by 124.5 km Data Domain, a conclusion is that over 10 days of data-driven forecasting, the open-boundary forcing has a significant impact on the Monterey Bay region. Uncertainties also exist in the atmospheric forcing. Although the general upwelling/relaxation cycles were well represented, the atmospheric uncertainties would primarily affect the details of the fields in the upper layers of the forecasts (e.g., the warm protrusion of the preceding paragraph).

### 3.2. Qualitative evaluation of forecast circulation and hydrographic features

As the AOSN-II predictive skill exercise proceeded, qualitative assessments were made with whatever data and images were

[6] A finding from AOSN-II is that the assimilation should account for faster diurnal and tidal cycles. For subsequent experiments, twice daily assimilation cycles were used.

Please cite this article as: Haley, P.J. Jr., et al., Forecasting and reanalysis in the Monterey Bay/California Current region for the Autonomous Ocean Sampling Network-II experiment. Deep-Sea Research II (2008), doi:10.1016/j.dsr2.2008.08.010

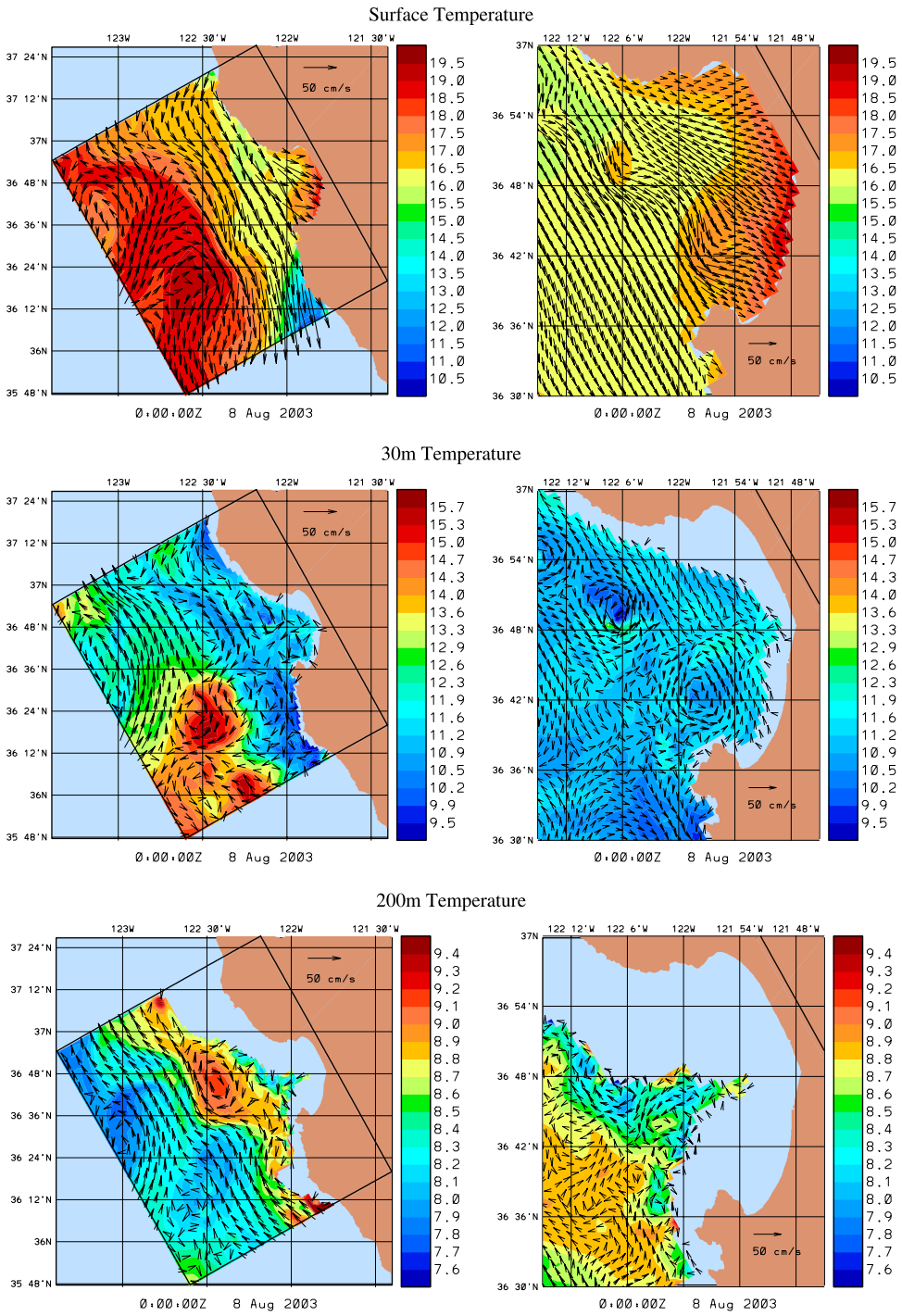


**Fig. 5.** Temperature (°C) and velocity (cm/s) fields for August 8, 2003 issued during the real-time exercise. These fields show the general structures that were observed in real-time.

available in real-time and reported.[7] A few of these real-time assessments are reproduced in Figs. 7 and 8, focusing on comparisons to SST and CODAR data. Comparing the HOPS surface temperature one-day forecast to NOAA POES AVHRR[8] on 12 August 2003 (left panels of Fig. 7), the model reproduces the general feature of an upwelling plume from the north being advected across the mouth of Monterey Bay and joining with the upwelling off PS. The model seems to advect more of the surface material to the south and fails to capture a westward extension of the plume by the northern edge of Monterey Bay. This is indicative of inaccuracies in the surface boundary layer parameters (they were in fact changed in real-time that week: see Lermusiaux, 2007) as well as inaccuracies in the atmospheric forcing fluxes. Surface properties are very sensitive to such parameters: for example, an error of 25% over a surface flow of 60 cm/s leads to an error of 13 km/day. On 13 August 2003 (middle panels of Fig. 7), a comparison of the surface temperature to aircraft SST (Ramp et al., 2009) still shows the cold plume across the mouth of the bay. Both the model surface temperature and the aircraft SST display warmer waters right at the coast of Monterey Bay, although the

[7] See the RTOC presentations in the local web site (Section 2.2).
[8] Courtesy of NWA and NOAA CoastWatch, http://coastwatch.noaa.gov/

Please cite this article as: Haley, P.J. Jr., et al., Forecasting and reanalysis in the Monterey Bay/California Current region for the Autonomous Ocean Sampling Network-II experiment. Deep-Sea Research II (2008), doi:10.1016/j.dsr2.2008.08.010

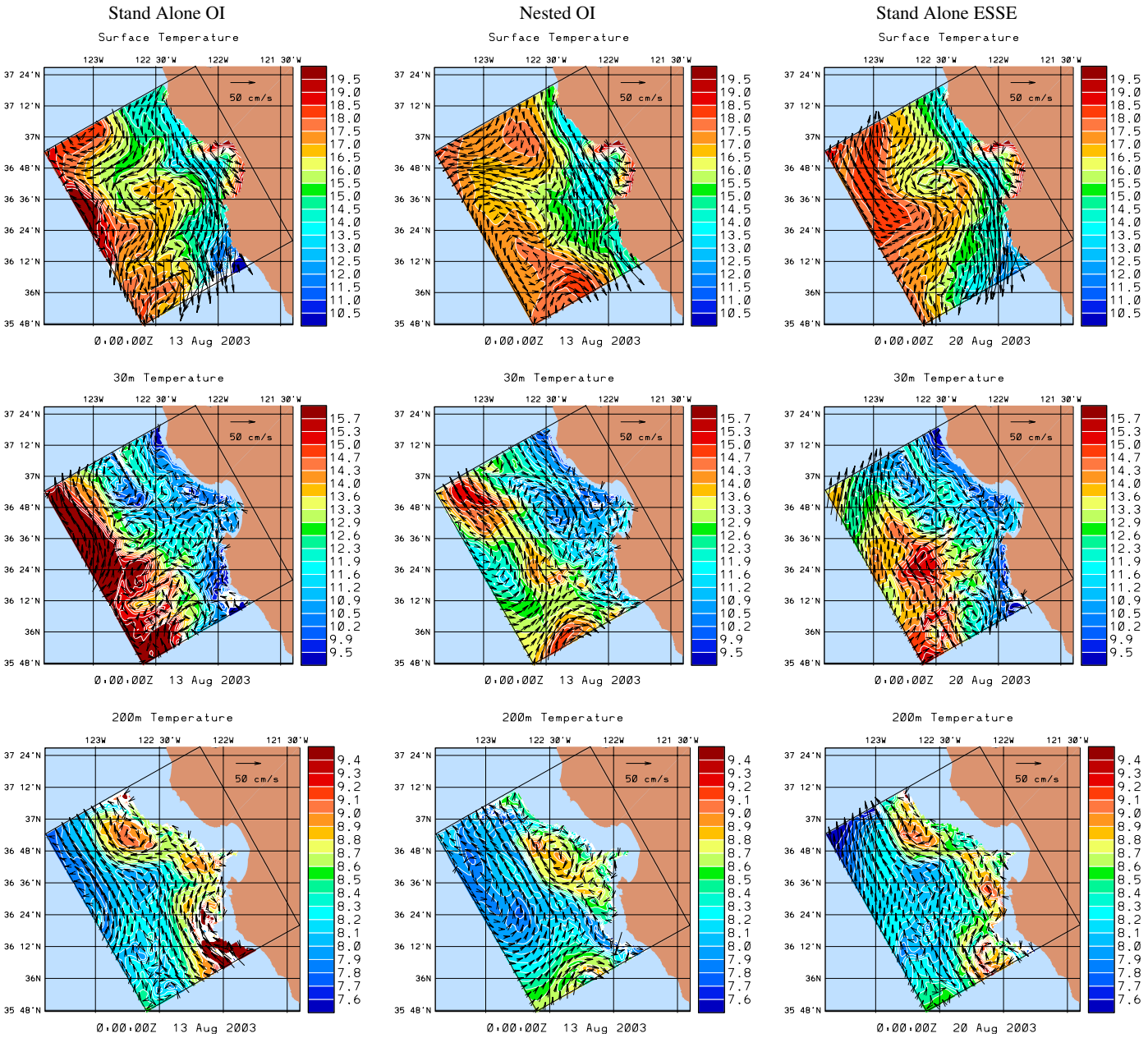


**Fig. 6.** Comparison of temperature (°C) and velocity (cm/s) for stand-alone, nested and ESSE forecasts for August 13, 2003.

model fields have these waters warmer and have a little warm water plume extending to the west out of the northern edge of Monterey Bay (lack of fog in atmospheric forcing and too geostrophic flow in the ocean model). Looking at the unobstructed portion of the NOAA POES AVHRR image from 21 August 2003 (right panels of Fig. 7) shows an elongated plume extending westward out of the southern edge of Monterey Bay, an upwelling center over PS and a wedge of warmer water separating them. The one-day forecast for 21 August 2003 captures the two cold pools separated by a warmer wedge. However, the westward extension of the plume is too short and the upwelling center off PS is displaced slightly to the south. In conclusion, the predicted surface temperature fields contain the dominant features but some of the smaller scales and more nonlinear phenomena were not well captured, especially to the west and south of the Bay, where observations were limited.

Fig. 8 shows the real-time comparisons between the available CODAR images (Paduan and Cook, 1997; Paduan and Lipphardt, 2003) and the HOPS forecasts. Note that both instantaneous and daily averaged CODAR images were used. This is because our primary concern was the general meso-scale circulation, which could be inferred from either type of image. The 19 August 2003 nowcast surface velocities show good qualitative agreement with the mapped CODAR data (left panels of Fig. 8). Both exhibit a southward flow across the mouth of Monterey Bay and a general cyclonic circulation within the bay. By 24 August (middle panels of Fig. 8), after the relaxation, the former cyclonic Bay circulation is no longer evident in either the CODAR nor the HOPS fields. The inflow in the Bay is captured well, as is the quiet northeast corner. The anti-cyclonic feature outside of the bay is not captured. By 30 August (right panels of Fig. 8), CODAR again shows a cyclonic circulation inside Monterey Bay, along with a southward flow at the southern end of Monterey Bay and a meandering southward flow offshore of Monterey Bay. All are well represented in the one-day forecast for 30 August. In conclusion, the assimilation of high-resolution WHOI glider data from the northern portion of the Bay

Please cite this article as: Haley, P.J. Jr., et al., Forecasting and reanalysis in the Monterey Bay/California Current region for the Autonomous Ocean Sampling Network-II experiment. Deep-Sea Research II (2008), doi:10.1016/j.dsr2.2008.08.010

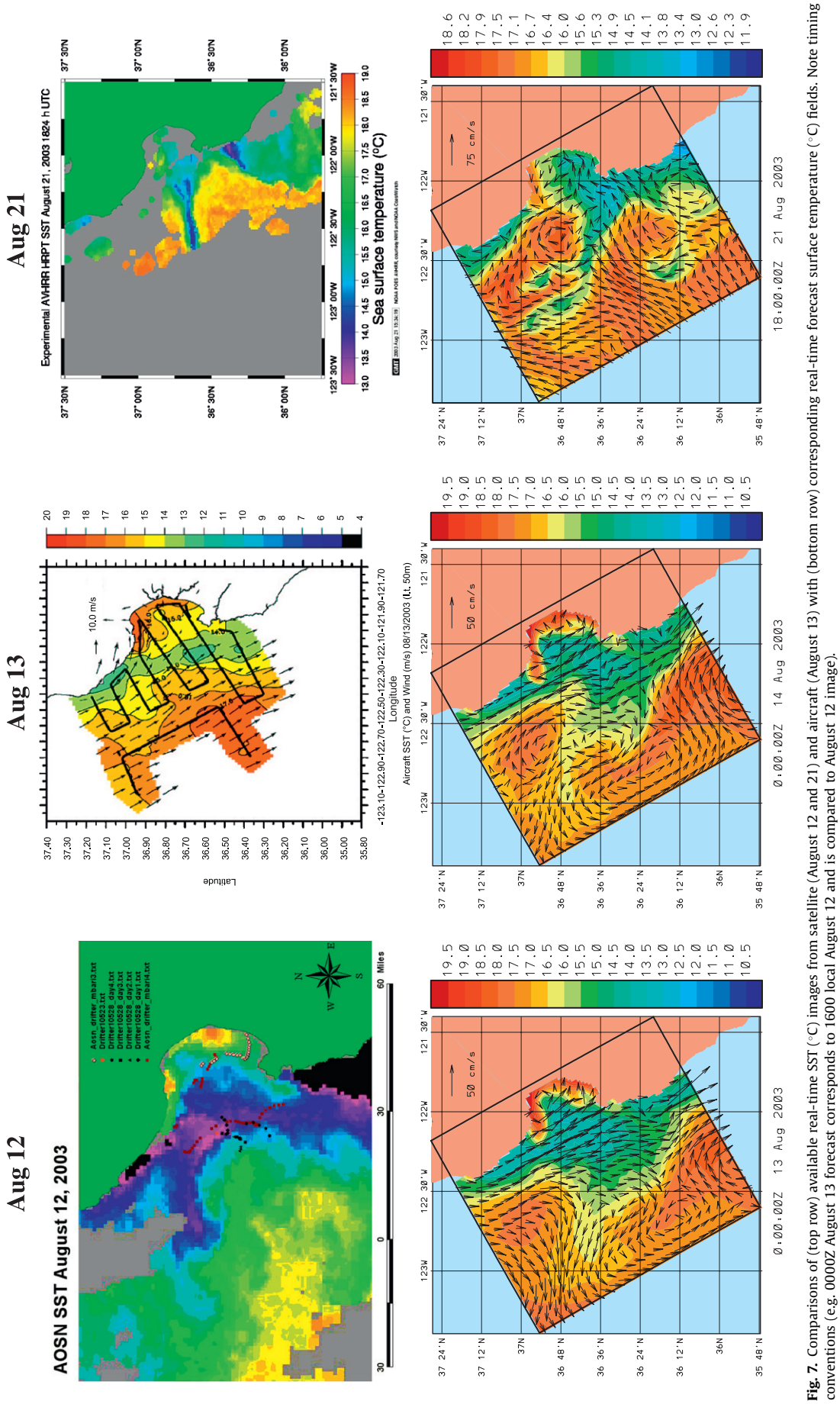


**Fig. 7.** Comparisons of (top row) available real-time SST (°C) images from satellite (August 12 and 21) and aircraft (August 13) with (bottom row) corresponding real-time forecast surface temperature (°C) fields. Note timing conventions (e.g. 0000Z August 13 forecast corresponds to 1600 local August 12 and is compared to August 12 image).

Please cite this article as: Haley, P.J. Jr., et al., Forecasting and reanalysis in the Monterey Bay/California Current region for the Autonomous Ocean Sampling Network-II experiment. Deep-Sea Research II (2008), doi:10.1016/j.dsr2.2008.08.010

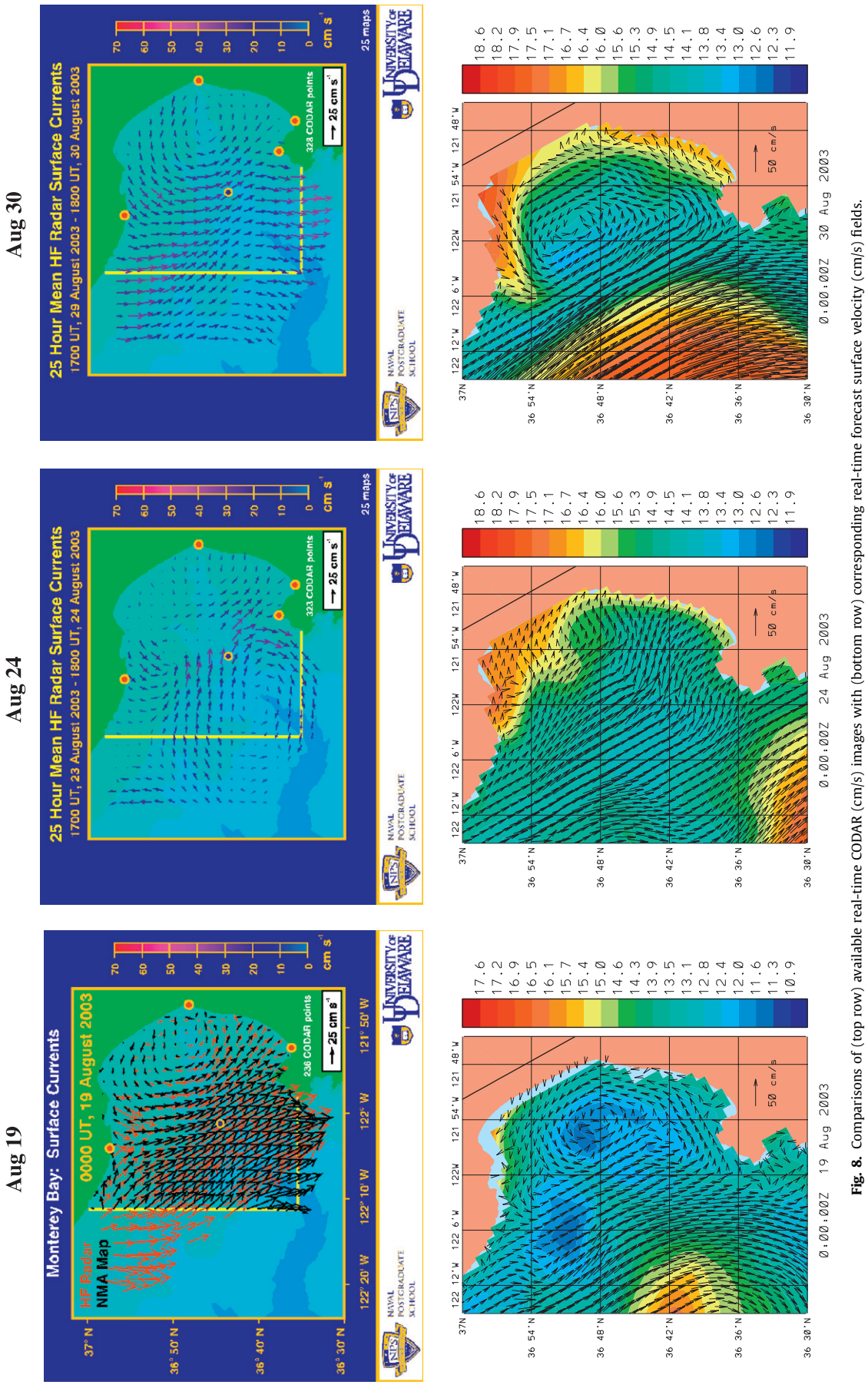


**Fig. 8.** Comparisons of (top row) available real-time CODAR (cm/s) images with (bottom row) corresponding real-time forecast surface velocity (cm/s) fields.

Please cite this article as: Haley, P.J. Jr., et al., Forecasting and reanalysis in the Monterey Bay/California Current region for the Autonomous Ocean Sampling Network-II experiment. Deep-Sea Research II (2008), doi:10.1016/j.dsr2.2008.08.010

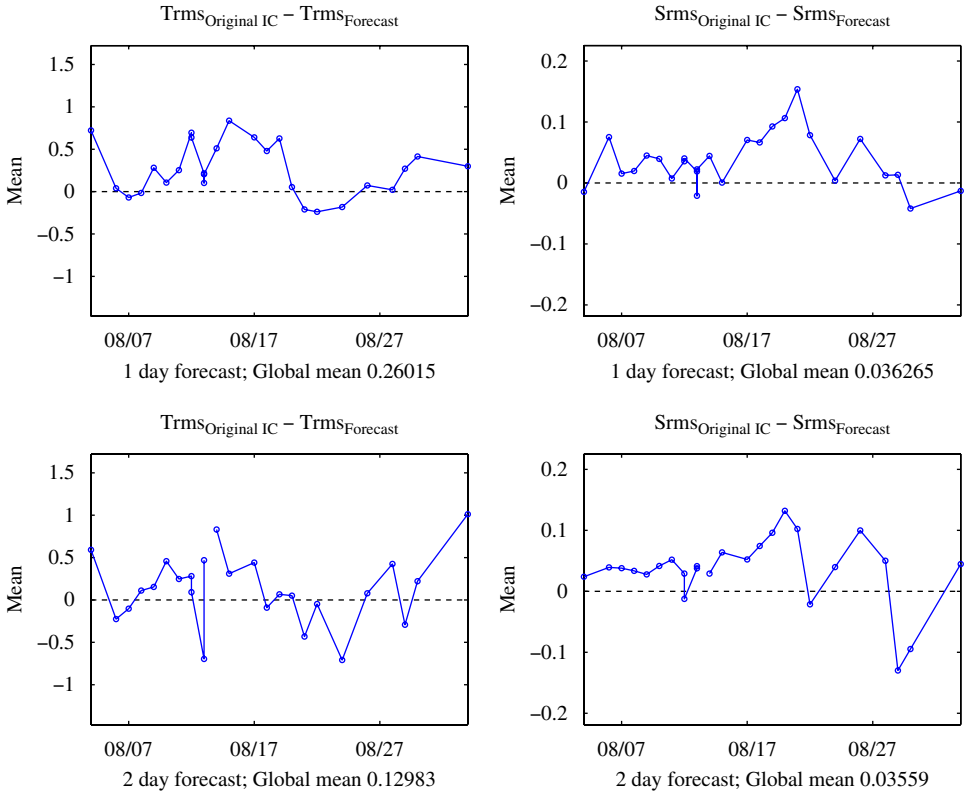


**Fig. 9.** Real-time volume-averaged RMS error differences. Persistence RMS—forecast RMS, a positive result indicates skill. The left column shows results for temperature (°C), the right for salinity (PSU). The top row shows results for one-day forecasts, the bottom row for two-day forecasts.

(see Fig. 3) leads to good predictions of the surface currents. This was encouraging since the ocean model utilized for AOSN-II did not yet contain tidal effects, which have non-zero mean effects on the hydrography and circulation.

Many other evaluations were carried out. One interesting one was carried by Marsden and his team at the California Institute of Technology (Chang, 2003). They used the HOPS forecast velocity fields to compute Lagrangian Coherent Structures (LCS) (Haller, 2002; Shadden et al., 2005, 2009; Lermusiaux and Lekien, 2005; Lermusiaux et al., 2006; Lermusiaux, 2006) in real-time (using ManGen[9]) and used these structures to predict the track of a drifter launched in Monterey Bay by Chavez at MBARI. The drifter always stayed on the same side of the predicted LCS separatrix, parallel to the mouth of the Bay at Point Pinos. This demonstrated that LCS are useful to characterize hyperbolic ocean features and that the HOPS surface current predictions were accurate enough to estimate the LCS. Admittedly, this was only a single event and therefore of limited probative value. However, it is usually the case that real-time operations have only limited (or even singular) opportunities for ancillary tests of the forecasting system.

### 3.3. Quantitative evaluation of forecast fields

To assess the predictive skill in the real-time forecasts, two skill metrics are introduced. The first is the root-mean-square error. Denoting the set of forecast values $\mathbf{T}_f$ and the corresponding set of observed values $\mathbf{T}_o$, then the root-mean-square forecast error, $\mathrm{Trms}_{\mathrm{Forecast}}$, is simply the root mean square of the difference between $\mathbf{T}_f$ and $\mathbf{T}_o$. Similarly the RMS persistence error, $\mathrm{Trms}_{\mathrm{Persistence}}$, is obtained by replacing the forecast values with the initialization values $\mathbf{T}_i$ in the root-mean-square difference. A forecast is said to have skill when the RMS forecast error is less than the RMS persistence error. A large number of skill studies were carried out. The illustrations shown below summarize the results.

Figs. 9–11 show differences between the RMS persistence errors and the RMS forecast errors for the one- and two-day forecasts of temperature and salinity issued in real-time. Each forecast is compared to *data not assimilated into the forecast*. These data are in the form of assimilation fields that were made after the forecast was issued, using data not available to the forecast. The comparisons were restricted to the regions where the non-dimensional observation OA error is less than or equal to 0.25. The RMSEs are computed at 2 m (surface), 10 m (base mixed layer/top of thermocline), 30 m (middle of thermocline), 150 m (CUC), 300 m (deep) and the mean of all the selected points on those levels. For a given forecast, persistence is defined as the particular initialization (Section 2.3.2) from which that forecast descends. That means that the comparison is to one of three sets of fields, depending on whether the simulation was made prior to August 7, between August 7 and 26 or after August 26.

Fig. 9 displays the temperature (in C) and salinity (in PSU) differences for the means at one- and two-day forecasts. On average, both temperature and salinity forecasts have skill out to two days. The average one-day temperature forecast shows greater skill than the two-day forecast (0.26 mean difference vs 0.13), whereas the salinity one- and two-day forecasts show equal skill (0.036 mean difference). The one-day forecast mean temperature differences show a correlation with the wind, having skill during the upwelling period of August 8–20 and a loss of skill during the relaxation period of August 21–24. A important contributing factor to this is the fact that the persistence being used in both periods comes from the data during the first R/V Pt. Sur survey. That survey was taken during the transition from a relaxation period to an upwelling period and is therefore much

[9] http://www.mangen.info/, see also Lekien et al. (2005).

Please cite this article as: Haley, P.J. Jr., et al., Forecasting and reanalysis in the Monterey Bay/California Current region for the Autonomous Ocean Sampling Network-II experiment. Deep-Sea Research II (2008), doi:10.1016/j.dsr2.2008.08.010

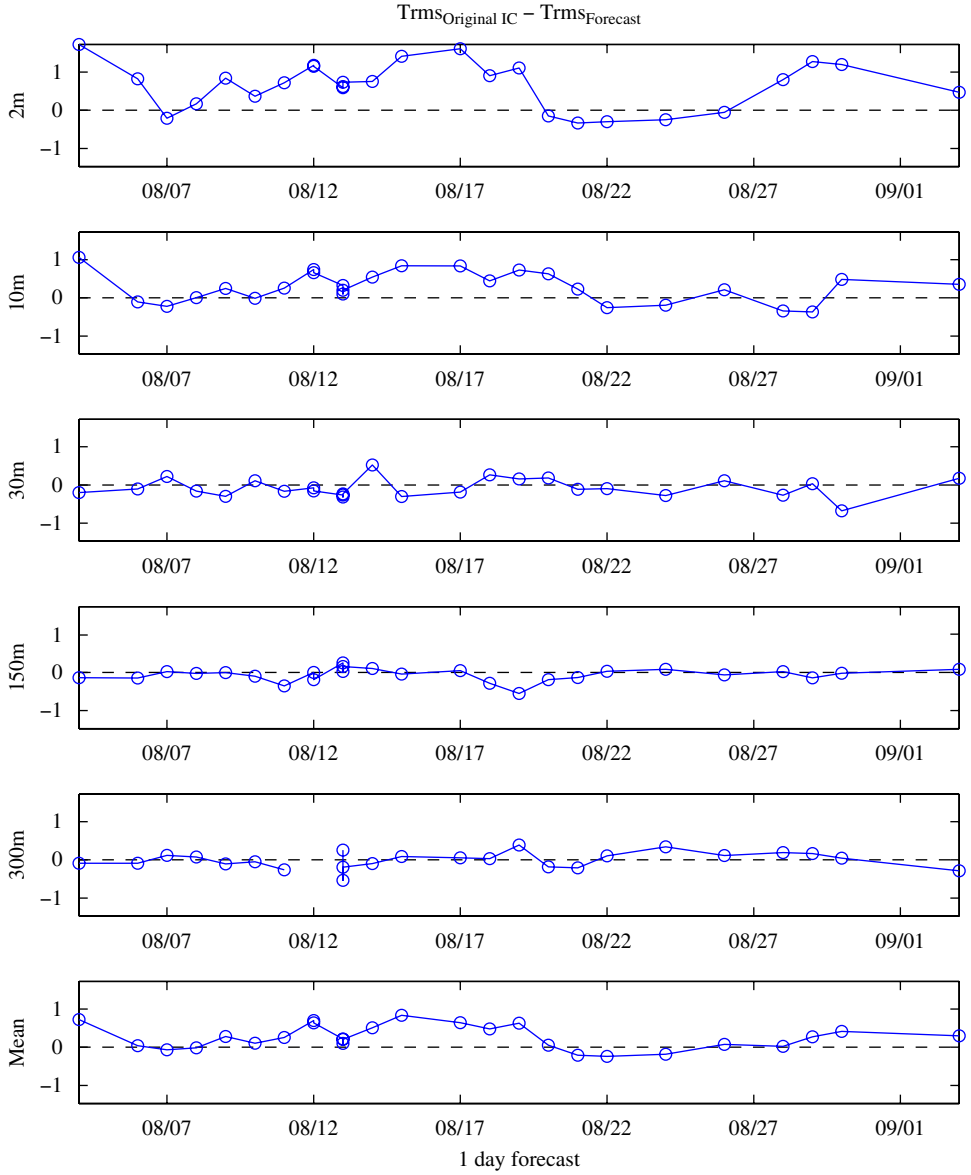


**Fig. 10.** Real-time temperature RMS differences (°C) for one-day forecasts. Persistence RMS—forecast RMS, a positive result indicates skill.

more similar to the second relaxation state than to the intervening upwelling state. Another factor is the impact of open-boundary uncertainties which become significant almost three weeks after the first larger-scale initialization survey and just before the second re-initialization.

Figs. 10 and 11 show the temperature RMS differences at all the computed levels for the one- and two-day forecasts, respectively. The temperature RMS shows greater skill and variability near the surface than at depth. A similar trend is found in salinity (not shown). At 30 m, the skill is increased after August 15 up to August 20 due to the updates in model parameters (see Lermusiaux, 2007). After that, the skill remains close to zero or is negative. This appears to be due to too coarse (3–5 m) vertical grid spacing offshore, near the bottom of the summer thermocline, to limited data assimilation at these depths because of issues with some of the real-time salinity data and to tidal effects which are neither part of the forecast nor the persistence. At deeper depths, the decreased variability and very limited data leads to skill estimates less accurate statistically. An interesting result is that forecast skill at 150 and 300 m remains positive about one week before the second initialization survey is available, while it does not at 30 m. This may be because below the thermocline, boundary uncertainties have not yet affected the larger-scale fields. The volume mean RMS differences most closely resembles the near surface differences. This reflects both the larger variations at the surface and the decreased number of data values at depth.

The second skill metric is the Pattern Correlation Coefficient (PCC) or Anomaly Correlation Coefficient. Using the notation for the RMS errors, the forecast PCC for temperature, Tpcc$_{\text{Forecast}}$, is given by

$$\text{Tpcc}_{\text{Forecast}} = \frac{(\mathbf{T}_f - \overline{\mathbf{T}_o})(\mathbf{T}_o - \overline{\mathbf{T}_o})^T}{\|\mathbf{T}_f - \overline{\mathbf{T}_o}\|\|\mathbf{T}_o - \overline{\mathbf{T}_o}\|} \quad (1)$$

In Eq. (1) the large-scale mean, $\overline{\mathbf{T}_o}$, is removed from every field. Hence, the PCC measures forecast skill based on the correlations of anomalies from this large-scale mean. In this work, $\overline{\mathbf{T}_o}$ is a weighted mean of the mapped observations, with the weighting

Please cite this article as: Haley, P.J. Jr., et al., Forecasting and reanalysis in the Monterey Bay/California Current region for the Autonomous Ocean Sampling Network-II experiment. Deep-Sea Research II (2008), doi:10.1016/j.dsr2.2008.08.010

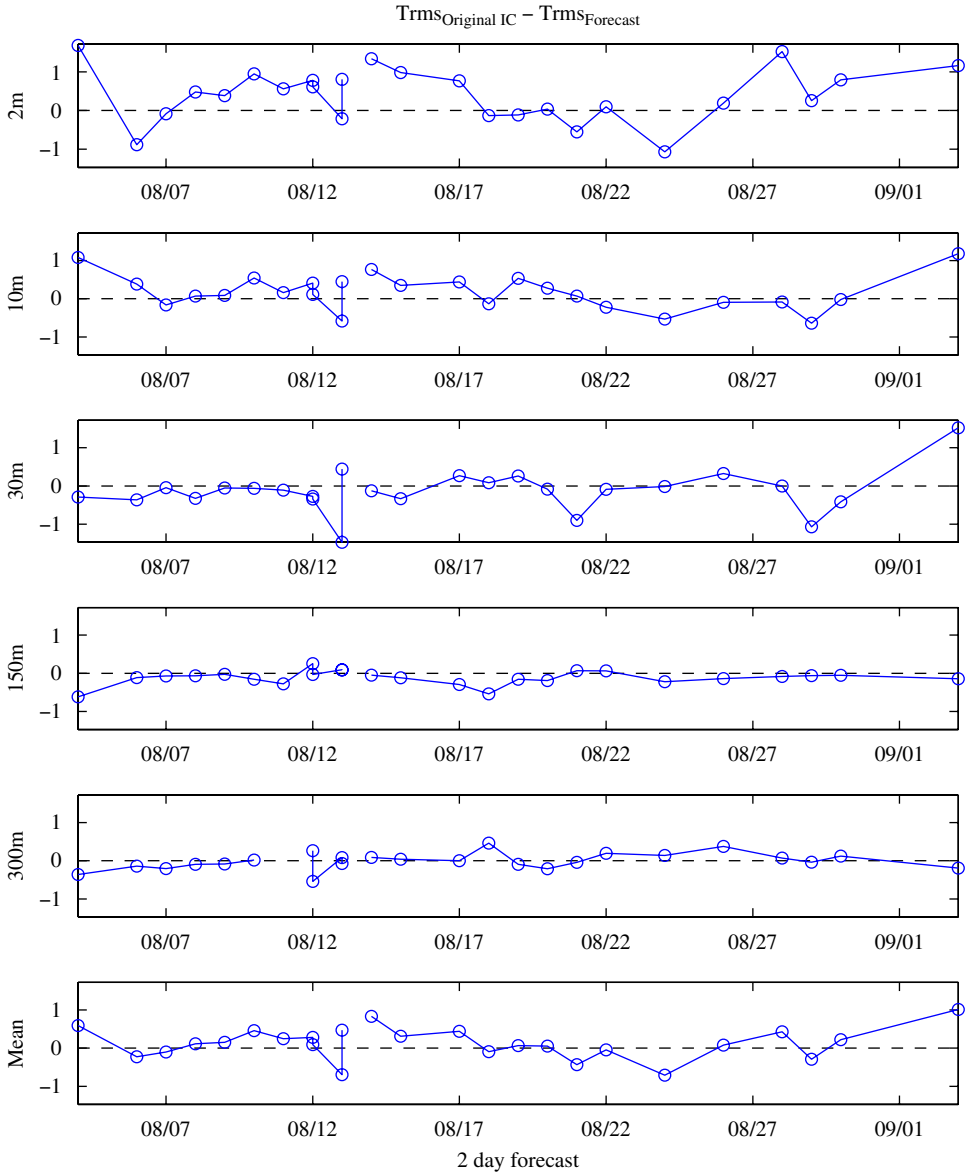


**Fig. 11.** Real-time temperature RMS differences (°C) for two-day forecasts. Persistence RMS—forecast RMS, a positive result indicates skill.

function $e^{-(r/45)^2}$ where $r$ is the distance (km) between an observation point and the point where the mean is being evaluated. This mean is computed each day, using only that day's mapped observations. The scaling in Eq. (1) is such that $\text{Tpcc}_{\text{Forecast}} \in [-1\ 1]$ with perfect correlation given by $\text{Tpcc}_{\text{Forecast}} = 1$, a complete lack of correlation given by $\text{Tpcc}_{\text{Forecast}} = 0$ and perfect anti-correlation given by $\text{Tpcc}_{\text{Forecast}} = -1$. As in the RMS error, the persistence PCC, $\text{Tpcc}_{\text{Persistence}}$, is obtained by replacing $\mathbf{T}_f$ with $\mathbf{T}_i$ in Eq. (1). Using PCC, a forecast is said to have skill if $\text{Tpcc}_{\text{Forecast}} > \text{Tpcc}_{\text{Persistence}}$.

Fig. 12 shows the mean PCC differences between the forecast and persistence for the issued real-time one- and two-day forecasts. As with the RMS errors, both temperature and salinity forecasts have, on average, skill out to two days. Here, the mean temperature PCC differences show similar skill at one and two days (~0.16 mean difference), while salinity shows greater skill at two days than 1 (0.072 mean difference at one day, 0.14 at two days). The depth dependence (not shown) is similar to the RMS error dependence, except for the fact that since PCC is already normalized, the PCC amplitudes do not decrease with depth. On average, PCC skills are better than RMS skills, which indicates that the simulation captures the mesoscale features relatively well.

## 4. Reanalysis methodology

The real-time forecasts present a series of realizations of the ocean in and around Monterey Bay. These realizations are, however, somewhat disjoint. This arises from three main sources: (1) different configurations (stand-alone OI, nested-OI and stand-alone ESSE) were employed for different forecasts (Fig. 6), (2) different starting and boundary conditions were employed at different times in the experiment (historical data and data based on the first and second R/V Pt. Sur cruises), and (3) model parameters were being tuned during the experiment. These differences prevent the real-time forecasts from being simply concatenated together and used for serious dynamical studies. In addition, quality control of the various datasets was completed during the year after the real-time exercise. Therefore a number of reanalyses of the AOSN-II data and forecasts were performed to

Please cite this article as: Haley, P.J. Jr., et al., Forecasting and reanalysis in the Monterey Bay/California Current region for the Autonomous Ocean Sampling Network-II experiment. Deep-Sea Research II (2008), doi:10.1016/j.dsr2.2008.08.010

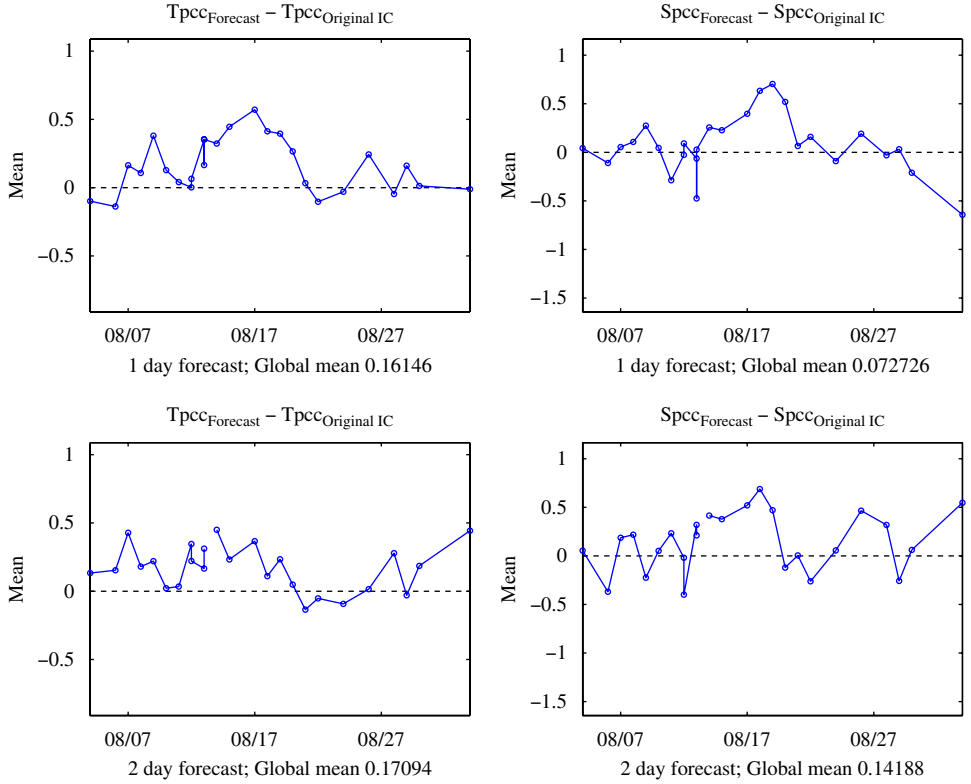


**Fig. 12.** Real-time volume-averaged PCC differences. Forecast PCC—persistence PCC, a positive result indicates skill. The left column shows results for temperature, the right for salinity. The top row shows results for one-day forecasts, the bottom row for two-day forecasts.

provide a single, continuous realization of the experiment. We next present the methodology of the final reanalysis.

The goal of the reanalysis is to produce a better tuned continuous four-dimensional representation of the oceans in the AOSN-II region with quality controlled data as well as numerical and dynamical parameter improvements. Because of the lack of offshore larger-scale data, the simplest configuration (stand-alone Data Domain with OI assimilation) is used first. To create the initial and open-boundary conditions, three OAs were made using the larger mesoscale "initialization" parameters in Table 1. The first was an analysis for 00Z on 6 August 2003 using R/V Pt. Sur CTDs, WHOI and SIO glider and NPS SST data in the period August 2–6, 2003. The second was an analysis for 00Z on August 23 using R/V Pt. Sur and R/V John Martin CTDs, WHOI and SIO glider and NPS SST data in the period August 21–25. The third was an analysis for 00Z on September 5 using R/V Pt. Sur CTDs in the period September 3–6. These analyses were then processed (with a level of no motion set to 1250 m) to produce initial condition fields and time-evolving boundary fields.

The boundary fields were used in the following manner. For temperature and salinity, the simulation boundary conditions were simply linear temporal interpolations of the analyses at the boundary, with persistence after September 5. For internal mode velocity, the time interpolated boundary data were used as the "larger-scale fields" in the boundary condition relaxation scheme (Appendix B). The transport streamfunction and barotropic vorticity used Orlanski radiation conditions.

Thirty-one assimilation fields were created from daily OAs of the August 6–September 6, 2003 hydrographic data collected by the R/Vs Pt. Sur, John Martin and Pt. Lobos; the WHOI and SIO gliders; and, the NPS aircraft SST. The correlation scales were those of Table 1 and analysis dates of August 7–September 6, at 1200Z. For each analysis, only data within ±18 h of the analysis time were used. From these mapped temperature and salinity fields, velocity first-guess estimates were obtained by geostrophic integration. Only the temperature, salinity and internal velocities were assimilated, following the schedule and weights of Table 2, with the provision that the weights for assimilating internal velocity were further reduced to half those in the table.

**Table 3**
AOSN-BC parameters used in real-time forecasts and reanalysis

| Boundary | $k_{fix}$ | $\tau_1$ (days) | $\tau_2$ (days) | $\gamma$ |
|---|---|---|---|---|
| Real-time values | | | | |
| *w* | 5 | 1 | 4 | 5 |
| *s* | 5 | 0.1 | 1.5 | 5 |
| *n* | 5 | 0.1 | 3.9 | 6 |
| Reanalysis values | | | | |
| *w* | 5 | 1 | 4 | 5 |
| *s* | 5 | 1 | 3.9 | 5 |
| *n* | 5 | 1 | 3.9 | 6 |

## 5. Reanalysis results

The main numerical result of the reanalysis is the improvement of the long-term robustness of the simulation, primarily by controlling instabilities in the southern boundary near PS. The three most important changes in this regard were: (1) the use of time-varying boundary data, described in Section 4; (2) additional smoothing of the topography in the neighborhood of PS, restricting the maximum slope to 0.11; and (3) weakening the

Please cite this article as: Haley, P.J. Jr., et al., Forecasting and reanalysis in the Monterey Bay/California Current region for the Autonomous Ocean Sampling Network-II experiment. Deep-Sea Research II (2008), doi:10.1016/j.dsr2.2008.08.010

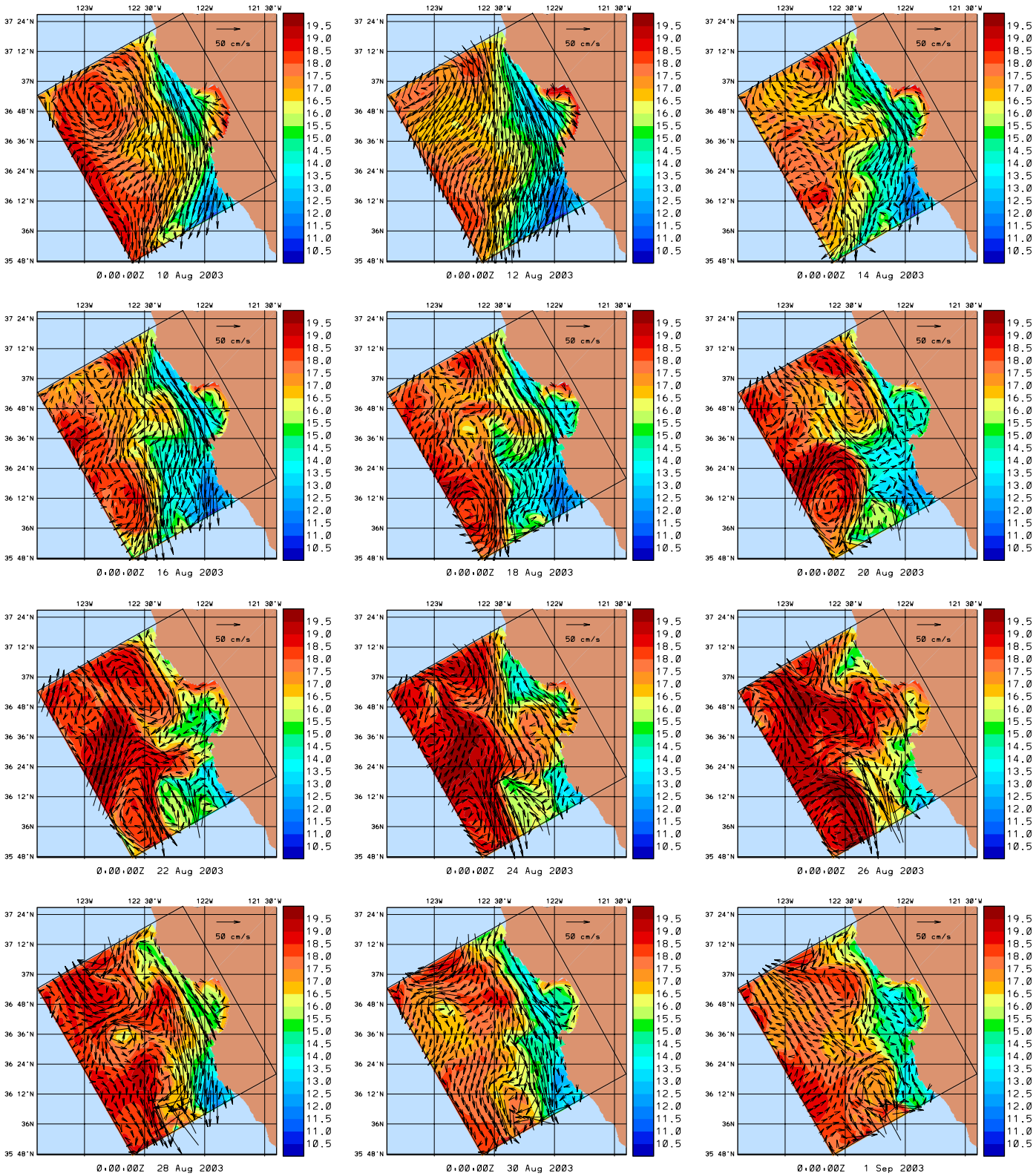


**Fig. 13.** Reanalysis surface temperature (°C) and velocity (cm/s) every two days for the period August 10–September 1, 2003.

relaxation parameters (Table 3) used in the boundary condition relaxation scheme. Additionally, to improve coastal currents, the coastal friction was weakened by increasing the relaxation time-scale (7200 s). Otherwise, the run parameters were the same as those used at the end of the real-time experiment.

Figs. 13 and 14 display the reanalysis temperature and velocity, at the surface and 30 m, respectively, every two days in the period 10 August–1 September 2003. The period August 10–16 is in a strong upwelling state. Both levels show a southward flowing coastal current which crosses the mouth of Monterey Bay and is

Please cite this article as: Haley, P.J. Jr., et al., Forecasting and reanalysis in the Monterey Bay/California Current region for the Autonomous Ocean Sampling Network-II experiment. Deep-Sea Research II (2008), doi:10.1016/j.dsr2.2008.08.010

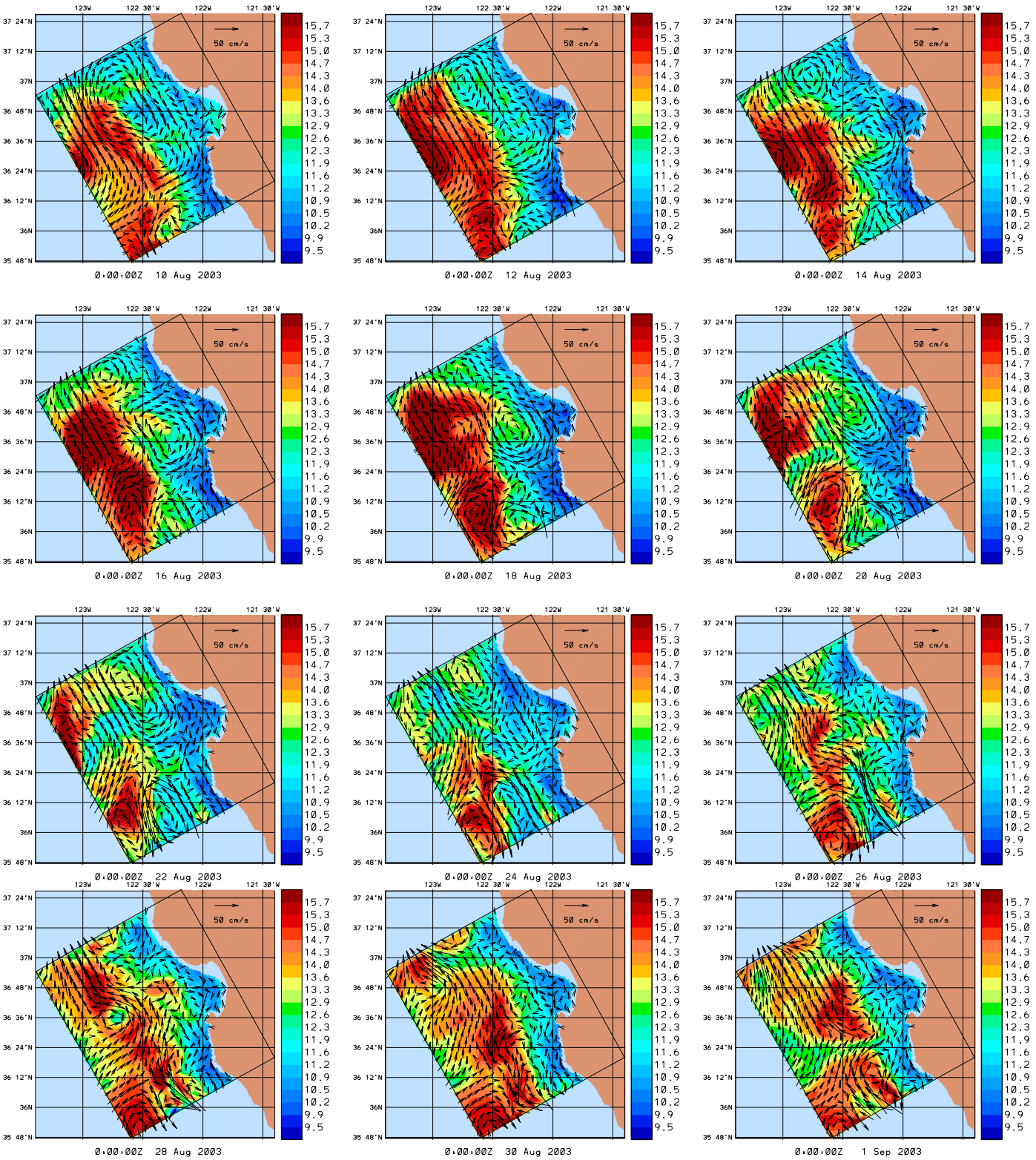


**Fig. 14.** Reanalysis 30 m temperature (°C) and velocity (cm/s) every two days for the period August 10–September 1, 2003.

deflected west (offshore) north of PS. The surface fields show upwelling plumes from points AN and Sur. The plume from AN extends south across the mouth of Monterey Bay and merges with the plume from PS by August 13. At 30 m, a broad flow enters the domain through the western boundary around 36°12′N and turns northwest. Along the northern shelf/slope, an elongated anticyclone spans the region between the southward coastal current and the northward offshore flow. This anticyclone retreats to the north while the offshore branch of the coastal current curves back and spins up another anticyclone, this time in the mouth of Monterey Bay. Overall, the circulation in the upper layers of the Bay is cyclonic during such upwelling conditions.

Please cite this article as: Haley, P.J. Jr., et al., Forecasting and reanalysis in the Monterey Bay/California Current region for the Autonomous Ocean Sampling Network-II experiment. Deep-Sea Research II (2008), doi:10.1016/j.dsr2.2008.08.010

The period 18–20 August is a transition between upwelling and relaxation states. The winds at M1 are generally weaker and their direction is more variable than before (Fig. 2). The upwelling at AN shuts down and the buoyancy flow patterns of the thermocline (30 m) begin to appear also at the surface. At 30 m the two previously described eddies propagate northward (the northern eddy passing through the domain entirely). The period August 22–26 is largely a relaxation state (with the 26th arguably more a transition day). The surface flows remain controlled by the thermocline flows. During this period in the real-time experiment, an apparent release of kinetic energy from the wind-driven surface mean circulation to internal mesoscale ocean features (including eddies and jets) was visualized and described by the ESSE uncertainty error fields (Lermusiaux, 2006). This mechanism was confirmed by the detailed multi-scale energy and vorticity dynamical analysis of the reanalysis fields by Liang and Robinson (2009).

During August 28–30, the winds are stronger again and in an upwelling configuration. The winds drive the surface flows and restart upwelling at point AN and PS. By September 1, winds die back down and the thermocline flows reassert control of the surface flows. An interesting characteristic to notice is that the upwelling patterns of the first and second upwelling are different. The first upwelling leads to wide westward plumes at the two

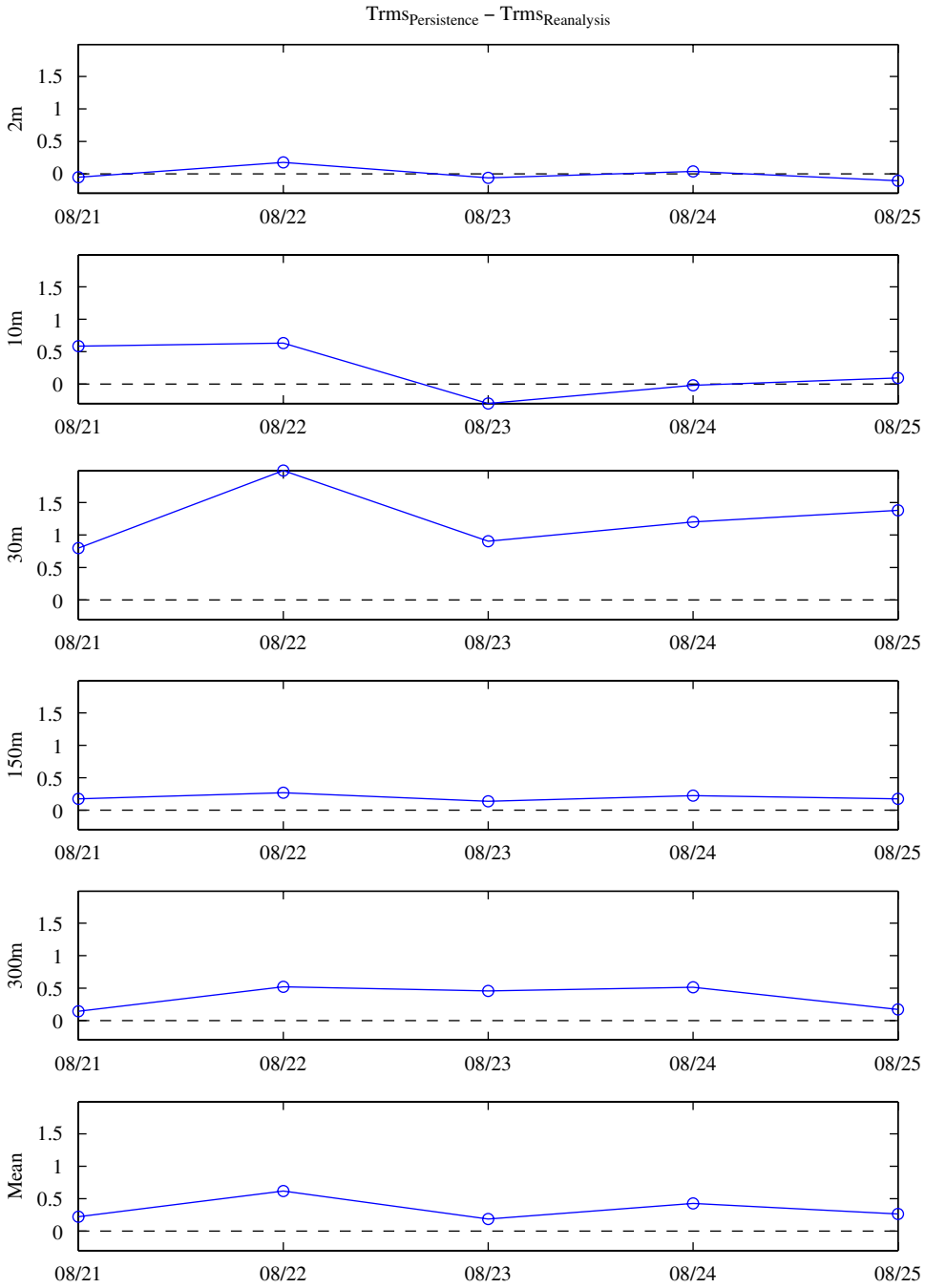


**Fig. 15.** Reanalysis temperature RMS differences (°C). Persistence RMS—reanalysis RMS, a positive result indicates skill. In this reanalysis simulation, only data up to August 20 was assimilated. Persistence is defined as the August 20 objective analysis of all data up to August 20.

Please cite this article as: Haley, P.J. Jr., et al., Forecasting and reanalysis in the Monterey Bay/California Current region for the Autonomous Ocean Sampling Network-II experiment. Deep-Sea Research II (2008), doi:10.1016/j.dsr2.2008.08.010

points, while the second does not. During August 28–30, the upwelling front is relatively parallel to the coast, just west of the mouth of Monterey Bay.

To assess the skill of the reanalysis, the simulation was repeated with the assimilation of data stopping on August 20. Skill metrics, as described in the real-time section, were then constructed comparing the repeat simulation to the fields that would have been assimilated on August 21–25 (corresponding to the second R/V Pt. Sur survey). For these comparisons, the persistence fields were constructed from a time dependent OA of all data prior to August 21 with an analysis date of August 20 (i.e. a "best, data only" estimate for 20 August). This persistence OA was made using the (larger) initialization scales (Table 1).

Fig. 15 shows the resulting differences in RMS errors between the temperature fields of the persistence and the above-described reanalysis simulation without data assimilation after August 20. For this reanalysis, the skill is positive at all depths and times, except on four instances. This is a large improvement when compared to the real-time forecast. It is the quality control of the ocean data and the improved model parameters, initial and boundary conditions that lead to this large improvement. The largest skill in amplitude mainly resides in the thermocline (30 m), which is the location of the largest dynamical variability during relaxation conditions. The skill at the surface is smaller in amplitude in part because of this. It is also smaller than for the real-time forecast because of the closer temporal proximity of the August 20 persistence fields to the new August 21–25 data.

A refined look at the vertical error structure was made by comparing the R/V Pt. Sur CTDs from the second survey to model-simulation profiles obtained by nearest-neighbor interpolation (space and time from August 21 to 25) from the persistence fields and the repeat reanalysis simulation fields (with no DA after August 20). These profiles were then vertically interpolated to a common 1 m vertical grid and differenced (simulation—data; persistence—data). These error profiles are then averaged over all profiles using either a simple mean (bias) or an root-mean-square estimate. The resulting mean temperature error profiles are presented in Fig. 16. Again, skill is seen in the main thermocline down to roughly the bottom of the CUC (300 m). At all of these dynamically active depths, the persistence "data-only" estimate is not as good as the model prediction. Below 300 m, there is a nearly linear increase in the bias down to 500 m, followed by a more gradual decrease. This loss of skill is due in part to the general lack of data below 400 m between the R/V Pt. Sur surveys (no glider data below 400 m and only intermittent small CTD surveys). Even though there is very little data to understand the cause of this deep drift of the model estimates, it could possibly be corrected by a better tuning of the deep model parameters.

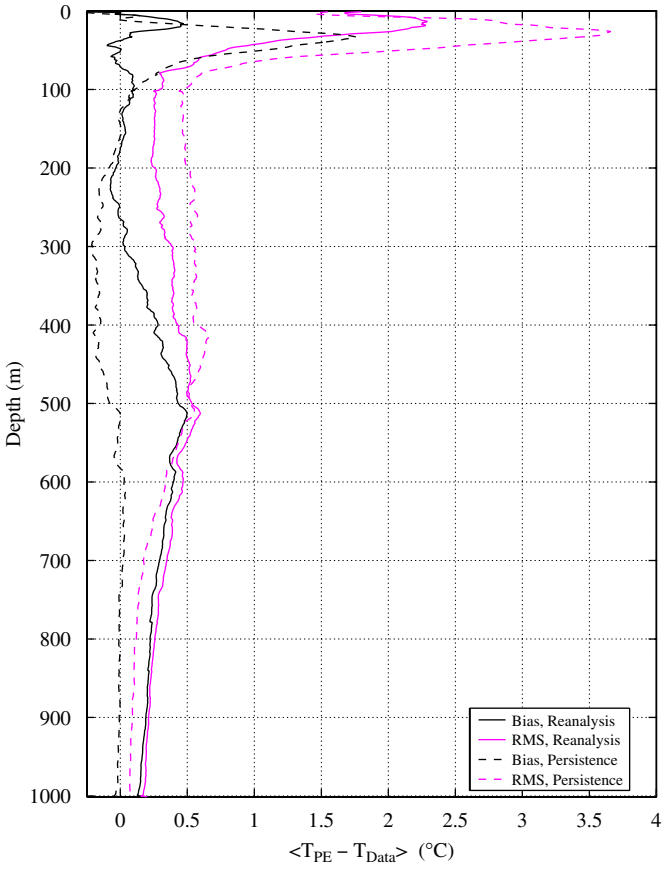


**Fig. 16.** Reanalysis temperature bias (°C) and RMS (°C) comparisons, averaged over August 21–25. In this reanalysis simulation, only data up to August 20 was assimilated. Persistence is defined as the August 20 objective analysis of all data up to August 20.

## 6. Conclusion

The methodologies and results of the utilization of HOPS during AOSN-II were presented and studied. These included a description of the modeling approach and modeling system components. The approach consisted of initializing the modeling system from adequate background ocean fields, which is often obtained from a synoptic survey of the larger-scale conditions in the region. Subsequently, data are assimilated, the model skill is evaluated and model properties are improved, all in real-time. Importantly, the model outputs are studied in as much details as possible within the time and personnel constraints, so as to foster real-time improvements in possibly all components of the modeling system.

During AOSN-II, conditions were on average in anomalously strong upwelling-favorable conditions. Two week-to-10-days long upwelling events were separated by two 3-to-5-days-long relaxation events. HOPS was re-initialized three times, once from historical data, twice from each of the first two R/V Pt. Sur surveys. The modeling system assimilated various data types (Ship CTD, AUVs, gliders and SST data) and model parameters were improved in real-time. From the real-time results, one can already obtain a description of several general circulation and hydrographic properties of the region that remained valid after reanalysis and model improvements.

The qualitative evaluation of the real-time forecast skill showed that many of the surface ocean features were predicted, but that their detailed position and shapes as well as their (sub)-mesoscale properties were often not accurate, especially offshore where data were limited. In the Bay, the match with surface velocity data (not assimilated) was on average good. This indicates that the WHOI gliders measuring the northern portion of the Bay allowed the estimation of the surface circulation over the whole Bay, even in the absence of tidal forcing. This was feasible because of the use of a data-assimilative ocean model, including the other datasets (see Fig. 3) and the atmospheric predictions. Note that the HOPS surface current predictions in the Bay also were found accurate enough to estimate the LCS in a very useful way for surface drifter planning and tracking.

The quantitative evaluation of the real-time forecast skill based on RMS error comparisons showed that the real-time forecasts had, on average, skill out to two days. The skill was found to be greater near the surface. The PCC comparisons showed, on average, greater skill than the RMS comparisons. This indicates that the mesoscale features were, overall, well represented in the real-time forecast.

Please cite this article as: Haley, P.J. Jr., et al., Forecasting and reanalysis in the Monterey Bay/California Current region for the Autonomous Ocean Sampling Network-II experiment. Deep-Sea Research II (2008), doi:10.1016/j.dsr2.2008.08.010

For simulations of 10 days or more in duration, it was found that uncertainties in the open-boundary forcing of our Data Domain could lead to significant errors in the Monterey Bay region.

The main results of the reanalysis effort is an improvement of the long-term stability of the simulation through improved model parameters and open-boundary conditions. These boundary conditions are based on a time-varying larger-scale objective analysis of observations. The quantitative skill of the reanalysis was also measured and improved when compared to the real-time fields. These reanalysis fields allowed a description of the significant ocean features that occurred during AOSN-II. Two types of upwelling events were observed, one with bifurcations or plumes extending westward at point AN and PS, and one with a thinner band of upwelled water parallel to the coast and across Monterey Bay. During strong upwelling events the flow in the upper 10–20 m has scales similar to atmospheric scales, with broad features. Once the winds subside, kinetic energy becomes available and leads to mesoscale features developing within a warming (relaxing) upper thermocline. The estimated flow at deeper 100–300 m depths consisted on average of an overall broad northward flow, sometimes with a branch following the coastal topographic features. Also simulated were the northward motions of the anticyclone and other eddies that often develop in front of Monterey Bay, and the westward plumes that develop in upwelling conditions.

A number of important lessons for future work were learned from this experiment. The first lesson was based on the existence of a strong daily cycle in the upper layers and on the shelf. To improve modeling this cycle, the data need to be assimilated more frequently, with shorter time groupings (e.g., twice daily assimilations, at the times of maximum/minimum observed SST, with correspondingly smaller time windows, Section 4 and Table 2, and correlation scales, Table 1). A second lesson was the importance of sufficient synoptic accuracy in the larger domain for two-way nesting. Feature models could be used to extend limited observations in a dynamically useful way for initialization of the larger domain. Output from another dynamical model (with sufficient accuracy) could be another source for initial/boundary conditions. A third lesson dealt with the specifics of the "Data Domain". A finer resolution near the thermocline was indicated by the evaluation of the real-time forecasts (Section 3.3). The prevalence of numerical issues at the southern boundary argued for moving south, to include the entire dynamic upwelling-center region in the numerical domain. A fourth lesson came from the results of the reanalysis, namely a continuous set of fields covering the experiment, and the improved skill that resulted. This could be realized in a real-time experiment by performing longer, full experiment sensitivity studies overnight (between the issuance of the products and the start of the next day's operations, Fig. 4). There is additional work and research remaining in studies of the AOSN-II data based on dynamical models. One also should investigate the effects of adding a hierarchy of ever more complex tidal parameterizations, from a simple increase of mixing coefficients as a function of barotropic tidal amplitudes to a full free surface simulations forced with barotropic tides (Rosenfeld et al., 2009; Wang et al., 2009). Some of the datasets which were not assimilated in the reanalysis presented could be used; they include buoy, CODAR (Shulman and Paduan, 2009) and SSH data. Learning from AOSN-II, most of these updates were carried out in August 2006 for the real-time Monterey Bay 06 experiment.

## Acknowledgments

We thank our colleagues from the AOSN-II team including A, Gangopadhyay, N. Leonard, J. Marsden, H. Schmidt, R. Davis, D. Fratantoni, I. Shulman, Y. Chao, S. Haddock, S. Majumdar, L. Rosenfeld and F. Lekien for useful discussions and fruitful collaborations. We are very greatful to our colleagues that have provided us with ocean measurements in real time, including R. Davis, D. Fratantoni, S. Haddock, M.A. McManus and E. McPhee-Shaw. We also thank the ship crews and other individuals involved in collecting ocean and atmosphere data. We thank J. Ryan and J. Paduan for providing us with high resolution topography for Monterey Bay. We thank D. Fratantoni for his work in editing this manuscript We also thank the three reviewers for their many useful comments. To carry out the present research, PJH, PFJL, WGL and OGL were supported by the Office of Naval Research under grants MURI-ASAP (N00014-04-1-0534, sub-00000917), ASRTP (N00014-07-1-0534) and core ONR6.1 (N00014-07-1-1061) to MIT. For the first part of this effort, PJH, PFJL, ARR, WGL, OGL and XSL were funded by the Office of Naval Research under grants MURI-ASAP (N00014-04-1-0534) and core ONR6.1 (N00014-05-1-0335) to Harvard University. J. Doyle acknowledges support through the Office of Naval Research's Program Element 0601153N. Computational resources were supported in part by the Fleet Numerical Meteorology and Oceanography Command. COAMPS is a registered trademark of the Naval Research Laboratory.

## Appendix A. Characteristics of the Real-time modeling system components and processing

Detailed characteristics of the components and processing of the real-time modeling system are described next. These include the modeling domains, data processing and analyses, atmospheric forcing and product dissemination. Parameterizations, parameters and data assimilation are discussed in Section 2.3.

### A.1. Domains, nesting, grids and bathymetry

The Data Domain was centered at (36.62N, 122.40W) with an $83 \times 96$ grid at 1.5 km resolution. The Off Shore Domain was centered at (36.18N, 123.59W) with an $83 \times 96$ grid at 4.5 km resolution. Both domains had 22 terrain-following vertical levels arranged in a double-sigma configuration (Haley, 1999) with 12 levels in the upper system and 10 in the lower. Two-way interprocess communications exchange information between the two model domains. Specifically, the Off Shore Domain in the region of overlap is replaced with information averaged from the Data Domain and the boundaries of the Data Domain are constrained by information interpolated from the updated Off Shore Domain.

To obtain a bathymetry for the domains, a 30 arc second topography was constructed a follows. First a 25-m gridded topography[10] (MBARI, 2000), covering 36.44–37.06N 122.51–121.78W was averaged to a 30 arc second grid. Outside this grid, elevations were obtained from the 30 arc second GLOBE[11] dataset (Hastings and Dunbar, 1999). Bathymetry outside the range of the MBARI dataset, but inside 35.52–37.99N 123.975–121.041W were obtained from a 0.01° dataset constructed by NPS.[12] Bathymetry outside of the range of the NPS dataset were taken from a 1-min DBDB-V[13] dataset (Steed et al., 2002).

[10] Provided by John Ryan.

[11] http://www.ngdc.noaa.gov/mgg/topo/globe.html

[12] "Derived from a combination of two sources: (1) Monterey Bay Aquarium Research Institute, Moss Landing, California and (2) U.S. Geological Survey, Menlo Park, California" Jeff Paduan, NPS (personal communication).

[13] https://128.160.23.42/dbdbv/dbvquery.html

Please cite this article as: Haley, P.J. Jr., et al., Forecasting and reanalysis in the Monterey Bay/California Current region for the Autonomous Ocean Sampling Network-II experiment. Deep-Sea Research II (2008), doi:10.1016/j.dsr2.2008.08.010

The resultant topography was then bilinearly interpolated to the horizontal grid of each domain. The interpolated topographies were then conditioned by: (1) resetting all depths shallower than 10 m to be 10 m; (2) applying a two-dimensional median filter (Lozano et al., 1994); and (3) applying a smoothing algorithm to simultaneously bound the reduced slope by 2.5 and the slope by 0.225 (Haley and Lozano, 2001).

### A.2. Oceanographic data processing and OAs

On a daily basis, the available CTD profiles and WHOI and SIO glider pseudo-profiles were collected and converted to the HOPS ASCII format. First, the data from each individual instrument were manually examined for internal consistency. When needed, a median filter (Tukey, 1977) was applied to de-spike noisy data. Then the profiles from different instruments were manually compared to each other and to the most recent R/V Pt. Sur CTD survey. Inconsistent data points were identified and removed. Every effort was made to retain as much data as possible (e.g., if a profile fell within the common envelope in its surface and deep values but was far off in the thermocline, only the thermocline portion would be removed.).

The *in situ* and SST profiles were gathered together and processed through the HOPS OA package. The data were then analyzed with the correlation parameters in Table 1, depending on whether the analyzed fields were to be used to initialize a simulation or to be assimilated into a simulation. The outputs of the OA were three-dimensional fields of temperature, salinity, dynamic height and their associated errors. These fields were located on the same horizontal grid as the PE domain, but were on flat levels in the vertical. The temperature and salinity were interpolated to the PE terrain-following vertical coordinates. The dynamic height was first differentiated to produce horizontal velocities on the flat levels. These velocities were then interpolated to the terrain-following coordinates, and decomposed into a depth averaged component and an "internal" (remainder) component. The depth averaged component was used to generate a transport streamfunction, to ensure the non-divergence of transport.

### A.3. Atmospheric forcing flux processing

The Navy's operational Coupled Ocean/Atmosphere Mesoscale Prediction System analysis and 72 h forecast fields (Doyle et al., 2009) were processed prior to their utilization. The wind-stress fields from COAMPS were bi-cubically interpolated to the HOPS grids, rescaled from ($N/m^2$) to ($dyne/cm^2$) and decomposed in terms of the direction vectors aligned with the HOPS grids. Special care was taken to resolve the mismatch of HOPS and COAMPS land masks. COAMPS wind-stress values are, on average, an order of magnitude higher over the land than over the sea. Hence, discrepancies in the land masks could lead to excessive values of the wind stress on the HOPS grids near the coasts. To control this problem, only wind stress values from COAMPS sea-points were used to interpolate/extrapolate to the HOPS grids.

The surface net heat flux into the ocean ($W/m^2$) was composed as the sum of the shortwave radiation, the longwave radiation, the sensible heat flux and the latent heat flux; all of which were directly available from the COAMPS output and bi-cubically interpolated to the HOPS grids.

The net surface-water flux out of the ocean (cm/day) was calculated as the difference of evaporation minus precipitation. Evaporation was obtained by dividing the COAMPS latent heat flux by the latent heat of evaporation. The latent heat of evaporation, $L_v$ (J/kg), was computed from the COAMPS air temperature, $T_{air}$ (°C), using the empirical formula $L_v = 2.5008(10^6) - 2.3(10^3)T_{air}$ (Gill, 1982, p. 607). The resulting evaporation was then converted from ($kg/(m^2\,s)$) to (cm/day). The total precipitation was obtained directly from COAMPS, merely needing a conversion from (mm in 12 h) to (cm/day). The net water flux was bi-cubically interpolated to the HOPS grids.

The validation of COAMPS reanalysis products for the Monterey Bay was examined by Kindle et al. (2002) using the Monterey Bay Aquarium Research Institute (MBARI) mooring wind measurements. A two-year time series of observed winds at MBARI moorings M1 and M2 were found to be in good agreement with the model outputs, both on the synoptic scale and for summer-time diurnal variability. During AOSN-II, we compared a two-week sequence of COAMPS wind forecasts (with lead times of 24, 48 and 72 h) to the observational data from MBARI moorings M1 and M2. The forecasts at all examined lead times had winds with a generally correct magnitude (±2 m/s), reproduced well the observed diurnal cycle at both M1 and M2, and consistently reproduced the observed strong wind and wind relaxation events.

### A.4. Product dissemination

Plots of the HOPS real-time nowcast/forecast fields were uploaded to a local web page (Section 2.2). The horizontal plots were provided at four depths, pre-selected based on the vertical structure of the historical data: surface, 10 m (base of mixed layer), 30 m (middle of thermocline), and 200 m (CUC region). Vertical sections were made coming out of points AN and Sur and out of the center of Monterey Bay. Additional links include special products, pre-experiment planning documents and post-experiment on-going analyses.

NetCDF output files from the issued HOPS PE forecasts were uploaded to the MBARI server (Section 2.2). Specially requested products were also served there (e.g., output for LCS analysis).

## Appendix B. New open-boundary conditions

The southern open boundary by PS was especially problematic and limiting to simulation duration. To handle this boundary, a variation on the standard Orlanski radiation condition was implemented and used in real-time (see also Lermusiaux, 2007). It is based on relaxing the predicted boundary values to a control field and is described next. Note that a set of open-boundary conditions that are variations of this Orlanski-relaxation theme have also been implemented and will be reported elsewhere.

### B.1. Orlanski and relaxation based open-boundary conditions

"Boundary condition relaxation" is a relaxation-type forcing applied to the predicted open-boundary values (e.g. by an Orlanski scheme). This forcing imposes a tunable and weak constraint towards some background conditions. Of course, these background conditions can change with time, for example due to a larger-scale buoyancy forcing. The basic form of this forcing is

$$u^{n+1}_{b,i,k} = ubc^{n+1}_{b,i,k} - \omega_{b,k}(u^{n-1}_{b,i,k} - u_{data_{b,i,k}}) \tag{2}$$

where $u$ is the variable whose boundary values are being sought, $b$ is the boundary index, $i$ is the along-boundary index, $k$ is the depth index, $ubc$ is the predicted boundary value, $u_{data}$ is some additional data for $u$ along the boundaries and $\omega_{b,k}$ is the relaxation weight. The relaxation weight is computed from

$$\omega_{b,k} = \frac{2\Delta t}{\tau_{1b} + \tau_{2b}[e^{\gamma_b((1-k)/(K-1))} - e^{-\gamma_b}]} \tag{3}$$

Please cite this article as: Haley, P.J. Jr., et al., Forecasting and reanalysis in the Monterey Bay/California Current region for the Autonomous Ocean Sampling Network-II experiment. Deep-Sea Research II (2008), doi:10.1016/j.dsr2.2008.08.010

where $\Delta t$ is the time step (s), $\tau_1$ is the base decay rate (s), $\tau_2$ is the depth decay rate (s), $\gamma$ is a non-dimensional depth decay factor, and $K$ is the total number of model levels. For model levels shallower than $K - k_{\text{fix}}$, the local velocity $u^{n-1}_{b,i,k}$ is examined and, if found to be outflow, the weight $\omega_{b,k}$ is multiplied by $\frac{1}{4}$. All of these parameters were tuned to our specific situation in AOSN-II and we expect that their values should be modified for other periods or regions.

## References


Bellingham, J.G., 2006. New challenges for ocean technology. Marine Technology Society Journal 40 (2), 139–140.

Bellingham, J.G., Zhang Y., 2005. Observing processes that vary in time and space with heterogeneous mobile networks. In: Proceedings of the International Workshop on Underwater Robotics for sustainable management of Marine Ecosystems and Environmental Monitoring, Genoa, Italy, pp. 9–16.

Bretherton, F.P., Davis, R.E., Fandry, C.B., 1976. A Technique for objective analysis and design of oceanographic experiments applied to MODE-73. Deep Sea Research 23, 559–582.

Brink, K.H., Beardsley, R.C., Niiler, P.P., Abbot, M., Huyer, A., Ramp, S., Stanton, T., Stuart, D., 1991. Statistical properties of near-surface flow in the California coastal transition zone. Journal of Geophysical Research 96 (C8), 14693–14706.

Bryan, K., 1969. A numerical method for the study of the circulation of the World Ocean. Journal of Computational Physics 4 (3), 347–376.

Carter, E.F., Robinson, A.R., 1987. Analysis models for the estimation of oceanic fields. Journal of Atmospheric and Oceanic Technology 4 (1), 49–74.

Chang, K., 2003. Taking the Oceans' Pulse, With Help From Robot Subs. The New York Times, September 30, 2003. Section F; Column 3; Science Desk, pp. 1–2.

Chao, Y., Li, Z., Farrara, J., McWilliams, J.C., Bellingham, J., Capet, X., Chavez, F., Choi, J.-K., Davis, R., Doyle, J., Fratantoni, D., Li, P., Marchesiello, P., Moline, M.A., Paduan, J., Ramp, S., 2009. Development, implementation and evaluation of a data-assimilative ocean forecasting system off the Central California Coast. Deep-Sea Research II, [doi:10.1016/j.dsr2.2008.08.011].

Charney, J.G., Fjortoft, R., Von Neumann, J., 1950. Numerical integration of the barotropic vorticity equation. Tellus 2 (5), 237–254.

Chavez, F.P., Collins, C.A., 2000. Studies of the California current system: present, past and future. Deep-Sea Research II 47 (5–6), 761–763.

Chavez, F.P., Barber, R.T., Kosro, P.M., Huyer, A., Ramp, S.R., Stanton, T., Rojas de Mendiola, B., 1991. Horizontal advection and the distribution of nutrients in the coastal transition zone off northern California: effects on primary production, phytoplankton biomass, and species composition. Journal of Geophysical Research 96 (C8), 14833–14848.

Chavez, F.P., Pennington, J.T., Herlien, R., Jannasch, H., Thurmond, G., Friederich, G.E., 1997. Moorings and drifters for real-time interdisciplinary oceanography. Journal of Atmospheric and Oceanic Technology 14 (5), 1199–1211.

Collins, C.A., Garfield, N., Paquette, R.G., Carter, E., 1996. Lagrangian Measurement of subsurface poleward flow between 38°N and 43°N along the West Coast of the United States during Summer, 1993. Geophysical Research Letters 23 (18), 2461–2464.

Collins, C.A., Pennington, J.T., Castro, C.G., Rago, T.A., Chavez, F.P., 2003. The California Current system off Monterey, California: physical and biological coupling. Deep-Sea Research II 50 (14–16), 2389–2404.

Curtin, T.B., Bellingham, J.G., 2001. Autonomous ocean-sampling networks. IEEE Journal of Oceanic Engineering 26 (4), 421–423.

Curtin, T.B., Bellingham, J.G., 2009. Progress toward autonomous ocean sampling networks. Deep Sea Research II, this issue, [doi:10.1016/j.dsr2.2008.09.005].

Curtin, T.B., Bellingham, J.G., Catipovic, J., Webb, D., 1993. Autonomous oceanographic sampling networks. Oceanography 6 (3), 86–94.

Cushman-Roisin, B., 1994. Introduction to Geophysical Fluid Dynamics. Prentice-Hall, Englewood Cliffs, NJ, 320pp.

Davis, R.E., Eriksen, C.E., Jones, C.P., 2002. Autonomous buoyancy-driven underwater gliders. In: Griffiths, G. (Ed.), The Technology and Applications of Autonomous Underwater Vehicles. Taylor and Francis, London, pp. 37–58.

Davis, R.E., Leonard, N., Fratantoni, D.M., 2009. Routing strategies for underwater gliders. Deep-Sea Research II, this issue, [doi:10.1016/j.dsr2.2008.08.005].

Davis, T.M., Countryman, K.A., Carron, M.J., 1986. Tailored acoustic products utilizing the NAVOCEANO GDEM (a generalized digital environmental model). In: Proceedings, 36th Naval Symposium on Underwater Acoustics, Naval Ocean Systems Center, San Diego, CA.

Doyle, J.D., Jiang, Q., Chao, Y., Farrara, J., 2009. High-resolution real-time modeling of the marine atmospheric boundary layer in support of the AOSNII field campaign. Deep Sea Research II, this issue, [doi:10.1016/j.dsr2.2008.08.009].

Fiorelli, E., Leonard, N.E., Bhatta, P., Paley, D.A., Bachmayer, R., Fratantoni, D.M., 2006. Multi-AUV control and adaptive sampling in Monterey Bay. IEEE Journal of Oceanic Engineering 31 (4), 935–948.

Fox, A.D., Maskell, S.J., 1995. Two-way interactive nesting of primitive equation ocean models with topography. Journal of Physical Oceanography 25 (12), 2977–2996.

Garfield, N., Collins, C.A., Paquette, R.G., Carter, E., 1999. Lagrangian exploration of the California Undercurrent, 1992–95. Journal of Physical Oceanography 29 (4), 560–583.

Gill, A.E., 1982. Atmosphere-Ocean Dynamics. Academic Press, New York. 662pp.

Haley, P.J., 1999. Grids user's guide. Harvard Open Ocean Model Reports, 54, Harvard University, Cambridge, MA.

Haley, P.J., Lozano, C.J., 2001. COND_TOPO: topography conditioning in Matlab ⟨http://oceans.deas.harvard.edu/HOPS/Cond_Topo/cond_topo.ps.gz⟩.

Haley, P.J., Lermusiaux, P.F.J., Leslie, W.G., Robinson, A.R., 1999. Harvard Ocean Prediction System (HOPS) ⟨http://oceans.deas.harvard.edu/HOPS/HOPS.html⟩.

Haller, G., 2002. Lagrangian coherent structures from approximate velocity data. Physics of Fluids 14 (6), 1851–1861.

Hastings, D.A., Dunbar, P.K., 1999. Global land one-km base elevation (GLOBE) digital elevation model, documentation, volume 1.0. Key to Geophysical Records Documentation (KGRD) 34, NOAA National Geophysical Data Center, 325 Broadway, Boulder, Colorado 80303, USA.

Hayward, T.L., Mantyla, A.W., 1990. Physical, chemical and biological structure of a coastal eddy near Cape Mendocino. Journal of Marine Research 48 (4), 825–850.

Hickey, B.M., 1998. Coastal oceanography of Western North America from the tip of Baja California to Vancouver Is. In: Brink, K.H., Robinson, A.R. (Eds.), The Sea, vol. 11. Wiley, Inc., New York, pp. 345–393.

Hodur, R.M., 1997. The Naval Research Laboratory's Coupled Ocean/Atmosphere Mesoscale Prediction System (COAMPS). Monthly Weather Review 125 (7), 1414–1430.

Huyer, A.E., 1983. Coastal upwelling in the California Current system. Progress in Oceanography 12 (3), 259–284.

Huyer, A., Barth, J.A., Kosro, P.M., Shearman, R.K., Smith, R.L., 1998. Upper-ocean water mass characteristics of the California Current, Summer 1993. Deep-Sea Research II 45 (8–9), 1411–1442.

Huyer, A., Kosro, P.M., Fleischbein, J., Ramp, S.R., Stanton, T., Washburn, L., Chavez, F.P., Cowles, T.J., Pierce, S.D., Smith, R.L., 1991. Currents and water masses of the Coastal Transition Zone off northern California, June to August, 1988. Journal of Geophysical Research 96 (8), 14809–14831.

Johnston, T.M.S., Cheriton, O.M., McManus, M.A., Pennington, J.T., Chavez, F.P., 2009. Thin phytoplankton layer formation at eddies, filaments and fronts in a coastal upwelling zone. Deep-Sea Research II, this issue, [doi:10.1016/j.dsr2.2008.08.006].

Kindle, J.C., Hodur, R.M., deRada, S., Paduan, J.D., Rosenfeld, L.K., Chavez, F., 2002. A COAMPS reanalysis for the Eastern Pacific: properties of the diurnal sea breeze along the central California coast. Geophysical Research Letters 29 (24), 2203–2206.

Kosro, P.M., Huyer, A., Ramp, S.R., Smith, R.L., Chavez, F.P., Cowles, T.L., Abbott, M.R., Strub, P.T., Barber, R.T., Jessen, P., Small, L.F., 1991. The structure of the transition zone between coastal waters and the open ocean off northern California, winter and spring 1987. Journal of Geophysical Research 96, 14707–14730.

Lekien, F., Coulliette, C., Mariano, A.J., Ryan, E.H., Shay, L.K., Haller, G., Marsden, J., 2005. Pollution release tied to invariant manifolds: a case study for the Coast of Florida. Physica D 210 (1–2), 1–20.

Leonard, N.E., Graver, J.G., 2001. Model-based feedback control of autonomous underwater gliders. IEEE Journal of Oceanic Engineering 26 (4), 633–645 (special issue on Autonomous Ocean-Sampling Networks).

Leonard, N.E., Paley, D.A., Lekien, F., Sepulchre, R., Fratantoni, D.M., 2007. Collective motion, sensor networks and ocean sampling. Proceedings of the IEEE 95 (1), 48–77.

Lermusiaux, P.F.J., 1997. Error subspace data assimilation methods for ocean field estimation: theory, validation and applications. Ph.D. Thesis, Harvard University, Cambridge, MA.

Lermusiaux, P.F.J., 1999. Data assimilation via error subspace statistical estimation. Part II: Middle Atlantic Bight shelfbreak front simulations and ESSE validation. Monthly Weather Review 127 (7), 1408–1432.

Lermusiaux, P.F.J., 2001. Evolving the subspace of the three-dimensional multiscale ocean variability: Massachusetts Bay. Journal of Marine Systems 29 (1-4), 385–422.

Lermusiaux, P.F.J., 2006. Uncertainty estimation and prediction for interdisciplinary ocean dynamics. Journal of Computational Physics 217 (1), 176–199.

Lermusiaux, P.F.J., 2007. Adaptive modeling, adaptive data assimilation and adaptive sampling. Physica D 230 (1–2), 172–196.

Lermusiaux, P.F.J., F., Lekien 2005. Dynamics and Lagrangian coherent structures in the ocean and their uncertainty. Extended abstract in dynamical system methods in fluid dynamics, Oberwolfach Workshop. In: Marsden, J.E., Scheurle, J. (Eds.), Mathematisches Forschungsinstitut Oberwolfach, July 31st–August 6th, 2005, Germany, pp. 19–20.

Lermusiaux, P.F.J., Robinson, A.R., Haley, P.J., Leslie, W.G., 2002. Advanced interdisciplinary data assimilation: filtering and smoothing via error subspace statistical estimation. In: Proceedings of The OCEANS 2002 MTS/IEEE Conference, Vol. 2 Holland Publications, pp. 795–802.

Lermusiaux, P.F.J., Chiu, C.-S., Gawarkiewicz, G.G., Abbot, P., Robinson, A.R., Miller, R.N., Haley, P.J., Leslie, W.G., Majumdar, S.J., Pang, A., Lekien, F., 2006. Quantifying Uncertainties in Ocean Predictions. Oceanography 19(1), 92–105.

Li, P., Chao, Y., Vu, Q., Li, Z., Farrara, J., Zhang, H., Wang, X., 2006. OurOcean—an integrated solution to ocean monitoring and forecasting. In: Proceedings of the 2006 Oceans Conference Boston, September 2006, pp. 1–6.

Liang, X.S., Robinson, A.R., 2009. Multiscale processes and dynamics for the Monterey Bay region circulation. Journal of Physical Oceanography, in press doi:10.1175/2008JPO3950.1.


Please cite this article as: Haley, P.J. Jr., et al., Forecasting and reanalysis in the Monterey Bay/California Current region for the Autonomous Ocean Sampling Network-II experiment. Deep-Sea Research II (2008), doi:10.1016/j.dsr2.2008.08.010

Lozano, C.J., Haley, P.J., Arango, H.G., Sloan, Q., Robinson, A.R., 1994. Harvard coastal/deep water primitive equation model. Harvard Open Ocean Model Reports, 52, Harvard University, Cambridge, MA.

Lozano, C.J., Robinson, A.R., Arango, H.G., Gangopadhyay, A., Sloan, N.Q., Haley, Jr., P.J., Anderson, L., Leslie, W.G., 1996. An interdisciplinary ocean prediction system: assimilation strategies and structured data models. In: Malanotte-Rizzoli, P. (Ed.), Modern Approaches to Data Assimilation in Ocean Modelling Elsevier Oceanography Series. Elsevier Science, The Netherlands, pp. 413–452.

Lynn, R.J., Simpson, J.J., 1987. The California Current system: the seasonal variability of its physical characteristics. Journal of Geophysical Research 92 (C12), 12947–12966.

Marchesiello, P., McWilliams, J.C., Shchepetkin, A., 2003. Equilibrium structure and dynamics of the California Current System. Journal of Physical Oceanography 33 (4), 753–783.

MBARI, 2000. Monterey Bay Multibeam Survey; Digital Data Series No. 3. ©2000 MBARI.

Orlanski, I., 1976. A simple boundary condition for unbounded hyperbolic flows. Journal of Computational Physics 21 (3), 251–269.

Pacanowski, R.C., Philander, S.G.H., 1981. Parameterization of vertical mixing in numerical models of Tropical Ocean. Journal of Physical Oceanography 11 (11), 1443–1451.

Paduan, J.D., Cook, M.S., 1997. Mapping surface currents in Monterey Bay with CODAR-type HF radar. Oceanography 10 (2), 49–52.

Paduan, J., Lipphardt, B., 2003. Coastal Ocean Dynamics Applications Radar (CODAR) Data. Autonomous Ocean Sampling Network (AOSN) 2003 Field Experiment. Monterey Bay Aquarium Research Institute. Retrieved August 2003, from ⟨http://aosn.mbari.org⟩.

Pierce, S.D., Smith, R.L., Kosro, P.M., Barth, J.A., Wilson, C.D., 2000. Continuity of the poleward undercurrent along the eastern boundary of the mid-latitude north Pacific. Deep-Sea Research II 47 (5–6), 811–829.

Ramp, S.R., Jessen, P.F., Brink, K.H., Niiler, P.P., Daggett, F.L., Best, J.S., 1991. The physical structure of cold filaments near Point Arena, California, during June 1987. Journal of Geophysics Research 96 (C8), 14,859–14,883.

Ramp, S.R., Paduan, J.D., Shulman, I., Kindle, J., Bahr, F.L., Chavez, F., 2005. Observations of upwelling and relaxation events in the Northern Monterey Bay during August 2000. Journal of Geophysical Research 110, C07013, doi:10.1029/2004JC002538.

Ramp, S.R., Davis, R.E., Leonard, N.E., Shulman, I., Chao, Y., Robinson, A.R., Marsden, J., Lermusiaux, P., Frantantoni, D., Paduan, J.D., Chavez, F., Bahr, F.L., Liang, S., Leslie, W., Li, Z., 2009. Preparing to predict: the Second Autonomous Ocean Sampling Network (AOSN-II) experiment in the Monterey Bay. Deep-Sea Research II, this issue, [doi:10.1016/j.dsr2.2008.08.013].

Robinson, A.R., 1999. Forecasting and simulating coastal ocean processes and variabilities with the Harvard Ocean Prediction System. In: Mooers, C.N.K. (Ed.), Coastal Ocean Prediction, AGU Coastal and Estuarine Studies Series. American Geophysical Union, pp. 77–100.

Robinson, A.R., Arango, H.G., Warn-Varnas, A., Leslie, W.G., Miller, A.J., Haley, Jr., P.J., Lozano, C.J., 1996. Real-time regional forecasting. In: Malanotte-Rizzoli, P. (Ed.), Modern Approaches to Data Assimilation in Ocean Modelling. Elsevier Oceanography Series, Elsevier Science, The Netherlands, pp. 377–412.

Robinson, A.R., Lermusiaux, P.F.J., Sloan, N.Q., 1998. Data assimilation. In: Brink, K.H., Robinson, A.R. (Eds.), The Sea: The Global Coastal Ocean, Volume 10: Processes and Methods. Wiley, New York, pp. 541–594.

Robinson, A.R., Haley, P.J., Lermusiaux, P.F.J., Leslie, W.G., 2002. Predictive skill, predictive capability and predictability in ocean forecasting. In: Proceedings of the The OCEANS 2002 MTS/IEEE Conference, Vol. 2 Holland Publications, pp. 787–794.

Rosenfeld, L.K., Schwing, F.B., Garfield, N., Tracy, D.E., 1994. Bifurcated flow from an upwelling center: a cold water source for Monterey Bay. Continental Shelf Research 14 (9), 931–964.

Rosenfeld, L., Shulman, I., Cook, M., Paduan, J., Shulman, L., 2009. Methodology for a regional tidal model evalution, with application to Central California. Deep-Sea Research II, this issue, [doi:10.1016/j.dsr2.2008.08.007].

Rudnick, D.L., Davis, R.E., Eriksen, C.C., Fratantoni, D.M., Perry, M.J., 2004. Underwater gliders for ocean research. Marine Technology Society Journal 38 (2), 73–84.

Scripps Institution of Oceanography, University of California, 1999. Physical, chemical and biological data. CalCOFI cruises 9802, 9803, 9804, 9805 and 9806. SIO Ref. 99-9, 160pp.

Shadden, S.C., Lekien, F., Marsden, J.E., 2005. Definition and properties of Lagrangian coherent structures from finite-time Lyapunov exponents in two-dimensional aperiodic flows. Physica D 212 (3–4), 271–304.

Shadden, S.C., Lekien, F., Paduan, J.D., Chavez, F.P., Marsden, J.E., 2009. The correlation between surface drifters and coherent structures based on high-frequency radar data in Monterey Bay. Deep-Sea Research II, [doi:10.1016/j.dsr2.2008.08.008].

Shapiro, R., 1970. Smoothing, filtering and boundary effects. Reviews of Geophysics and Space Physics 8 (2), 359–387.

Sherman, J., Davis, R.E., Owens, W.B., Valdes, J., 2001. The autonomous underwater glider ''Spray''. IEEE Journal of Oceanic Engineering 26 (4), 437–446 (special issue on Autonomous Ocean-Sampling Networks).

Shulman, I., Paduan, J.D., 2009. Assimilation of HF radar-derived radials and total currents in the Monterey Bay area. Deep-Sea Research II, this issue, [doi:10.1016/j.dsr2.2008.08.004].

Shulman, I., Wu, C.R., Lewis, J.K., Paduan, J.D., Rosenfeld, L.K., Kindle, J.C., Ramp, S.R., Collins, C.A., 2002. High resolution modeling and data assimilation in the Monterey Bay area. Continental Shelf Research 22 (8), 1129–1151.

Shulman, I., Rowley, C., Anderson, S., DeRada, S., Kindle, J., Martin, P., Doyle, J., Cummings, J., Ramp, S., Chavez, F., Fratantoni, D., Davis, R., 2009. Impact of glider data assimilation on the Monterey Bay model. Deep-Sea Research II, this issue, [doi:10.1016/j.dsr2.2008.08.003].

Sloan III N.Q., 1996. Dynamics of a shelf-slope front: process studies and data-driven simulations in the Middle Atlantic Bight. Ph.D. Thesis, Harvard University, Cambridge, MA.

Spall, M.A., Holland, W.R., 1991. A nested primitive equation model for oceanic applications. Journal of Physical Oceanography 21 (2), 205–220.

Spall, M.A., Robinson, A.R., 1989. A new open ocean, hybrid coordinate primitive equation model. Mathematics and Computers in Simulations 31 (3), 241–269.

Steed, C.A., Braud, J.E., Koehler, K.A., 2002. VGRID: a generic, dynamic HDF5 storage model for georeferenced grid data. In: Oceans'02 MTS/IEEE, vol. 2, pp. 900–907.

Strub, P.T., James, C., 2000. Altimeter-derived variability of surface velocities in the California Current system: 2. seasonal circulation and eddy statistics. Deep-Sea Research II 47 (5–6), 831–870.

Strub, P.T., Kosro, P.M., Huyer, A., 1991. The nature of the cold filaments in the California Current system. Journal of Geophysical Research 96 (C8), 14743–14768.

Traganza, E.D., Conrad, J.C., Breaker, L.C., 1981. Satellite observations of a cyclonic upwelling system and giant plume in the California Current. In: Richards, F.A. (Ed.), Coastal Upwelling, DOE Symposium on Coastal Upwelling. AGU, pp. 228–241.

Tukey, J.W., 1977. Exploratory Data Analysis. Addison-Wesley. Reading, MA, 688 pp.

Wang, P., Song, Y.T., Chao, Y., Zhang, H., 2005. Parallel computation of the Regional Ocean Modeling System. The International Journal of High Performance Computing Applications 19 (4), 375–385.

Wang, X., Chao, Y., Dong, C., Farrara, J., Li, Z., McWilliams, J.C., Paduan, J.D., Rosenfeld, L.K., 2009. Modeling tides in Monterey Bay, California. Deep-Sea Research II, this issue, [doi:10.1016/j.dsr2.2008.08.012].

Wickham, J.B., 1975. Observations of the California countercurrent. Journal of Marine Research 33 (3), 325–340.

Please cite this article as: Haley, P.J. Jr., et al., Forecasting and reanalysis in the Monterey Bay/California Current region for the Autonomous Ocean Sampling Network-II experiment. Deep-Sea Research II (2008), doi:10.1016/j.dsr2.2008.08.010